Workshop of
CODE_BRIGHT USERS

19 April 2023
Barcelona, Spain
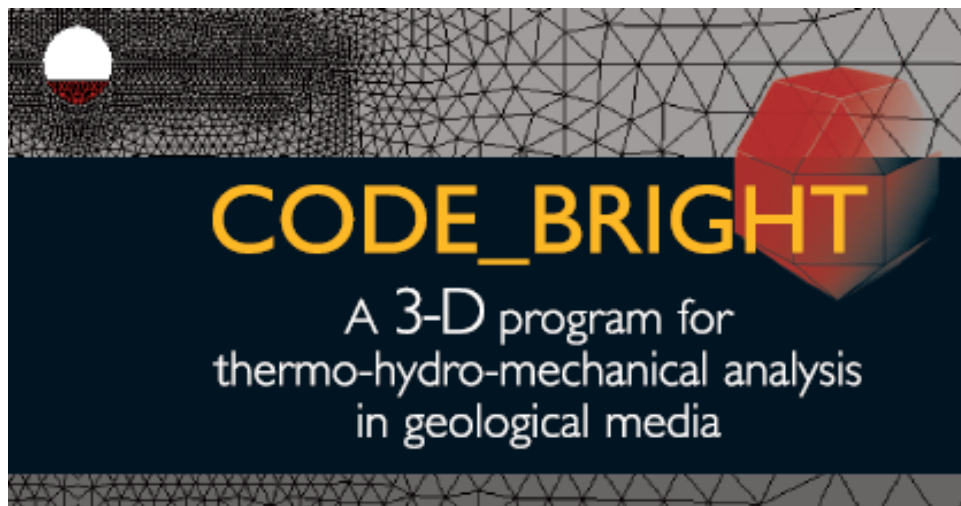
Department of Civil and Environmental Engineering
UPC-BarcelonaTech
Barcelona, Spain

CIMNE
International Center for Numerical Methods in Engineering
Barcelona, Spain

CODE_BRIGHT

A 3-D program for thermo-hydro-mechanical analysis in geological media

WORKSHOP OF CODE_BRIGHT USERS

Barcelona, 19 April 2023

Department of Civil and Environmental Engineering

(UPC-BarcelonaTech, Barcelona, Spain)

CIMNE

(International Center for Numerical Methods in Engineering, Barcelona, Spain)

CONTENTS

Modelling of Gas injection Tests in Clay Barriers, Laboratory to Field-Scale.

Erdem Toprak* and Sebastia Olivella*

*Department of Civil and Environmental Engineering Technical University of Catalonia (UPC), International Center for Numerical Methods in Engineering (CIMNE), Barcelona, Spain
E-mail: erdem.toprak@upc.edu; E-mail: sebastia.olivella@upc.edu

Key words: Gas injection tests on FEBEX, gas injection tests on COx, gas migration in clay barriers, EURAD-Gas project

Abstract:. The performance of different type of buffer or backfill materials (FEBEX and COx) in terms of gas transport capacity have been investigated by means of modelling of laboratory and/or full scale experiments. Modelling of laboratory and/or field-scale gas injection tests have been performed under different geometrical approaches that includes full 3D models and reduced 3D models. A set of sensitivity analyses (geological conditions, numerical simulation options and design options) has been proposed to provide a satisfactory reproduction of the experimental data. An initial heterogeneity has been incorporated to model geometries in a random way to simulate zones that have variable permeabilities. These modelling activities have been partly reported in EURAD-Gas Projects under Task 2 and Task 3.

1 INTRODUCTION

In the repository gas will be generated by several mechanisms, such as the anaerobic corrosion of metals, the microbial degradation of organic wastes and the radiolysis of water, which generate hydrogen, oxygen, methane and carbon dioxide. In the case of the engineer barriers, gas transport could take place mainly through preferential pathways, like the joints between compacted bentonite blocks, interfaces between different components or along the interface between host rock and buffer material. Once breakthrough pressure is reached, preferential pathways will be created. The size of these pathways would depend on gas local pressure and structural clay restrictions. These pathways would close once gas pressure decrease below a certain value, known as residual pressure. Meanwhile, gas pressure will increase again at the interface up to a new threshold pressure. Therefore, the gas generated will be transported outwards in a cyclic manner, regulated by the opening and closure of pathways, which will depend on the pressure reached [1]. In order to understand gas transport mechanism in clay barriers, several gas injection tests with different configurations have been modelled.

There are two modelling work has been discussed in this document:

- EURAD Task 2: Hydro-mechanical modelling of gas breakthrough tests on FEBEX material [2]: Mechanical understanding of gas transport in clay-based materials. In order to understand gas migration from bentonite barrier (FEBEX bentonite) also gas pathway development along the barrier; hydro-mechanical simulation of gas breakthrough tests [1] have been performed.
- EURAD Task 3: Hydro-mechanical modelling of PGZ Tests [3]: -In order to understand gas transport processes from engineered barrier system to host rock (gas migration mechanism into COx) by means of modelling of field-scale gas injection experiments. Several PGZ field-scale experiments [2] with different configurations have been modelled.

2 MODELLING RESULTS

EURAD Task 2: Hydro-mechanical modelling of gas breakthrough tests on FEBEX material

GID as a CAD system and Code_Bright as a Finite Element Method (FEM) program have been used in order to simulate gas breakthrough tests (Figure 1-A) in FEBEX bentonite material.

The sample (FEBEX bentonite) diameter is 38 mm and initial height of the sample is 20 mm. Initial saturation degree of the material is 81% which corresponds to initial water content of 15.3%. The test has been performed under constant volume.

The model has a 3D full geometry where porous stones have been simulated as separate materials (Figure 1-B). The geometry has structured mesh and the number of hexahedra elements is 960. There are 1197 nodes.

The injector system have been introduced to system as a boundary condition. Pre-escribed gas pressure have been applied from one end of the sample in the model. The sample has been saturated during 60 days. After reaching the full saturation, gas injection takes place till breakthrough pressure. When the second breakthrough happens, the gas pressure source is closed. Table 1 and Figure 1-C summarizes the processes taking place in the test.

Barcelona Basic Model (BBM) has been used as mechanical model. Cubic law for permeability (increase in permeability according gas injection) has been used as hydraulic model. Details of hydro-mechanical model parameters can be found in [3].

Table 1. Test interval data and comparison of back-pressures.

Steps of breakthrough tests	Description	Duration (d)	Back pressure Test	Back Pressure Model
Phase I	Saturation of the sample	60	-	-
Phase II	Gas injection - first BT	60	2.2	4.5
	Gas injection - second BT	80	1.7	4.5
Phase III	Dismantling of the sample and re-saturation	60	-	-
Phase IV	Gas injection - first BT	50	3.5	3.5
	Gas injection - second BT	50	3.4	3

Gas pressure evolution upper and lower part of the sample is shown in Figure 1-C. In Model, back pressure value in Phase IV (first BT) is around 3.5 MPa which is consistent with the test data (Table 1). However, the model slightly overestimates back pressure in Phase II. Figure 1-D shows the permeability increases during the gas injection steps in preferential pathways. The increase in permeability is concentrated mainly in the upper (gas entry) and lower (gas outlet) parts of the preferential pathways. During the gas injection, permeability increased because of aperture of fractures. Once the gas injections stopped, these apertures were closed so that permeability decreased.

Test set-up (BT test on FEBEX)	Model configuration
(A)	(B)

(C)

(D)
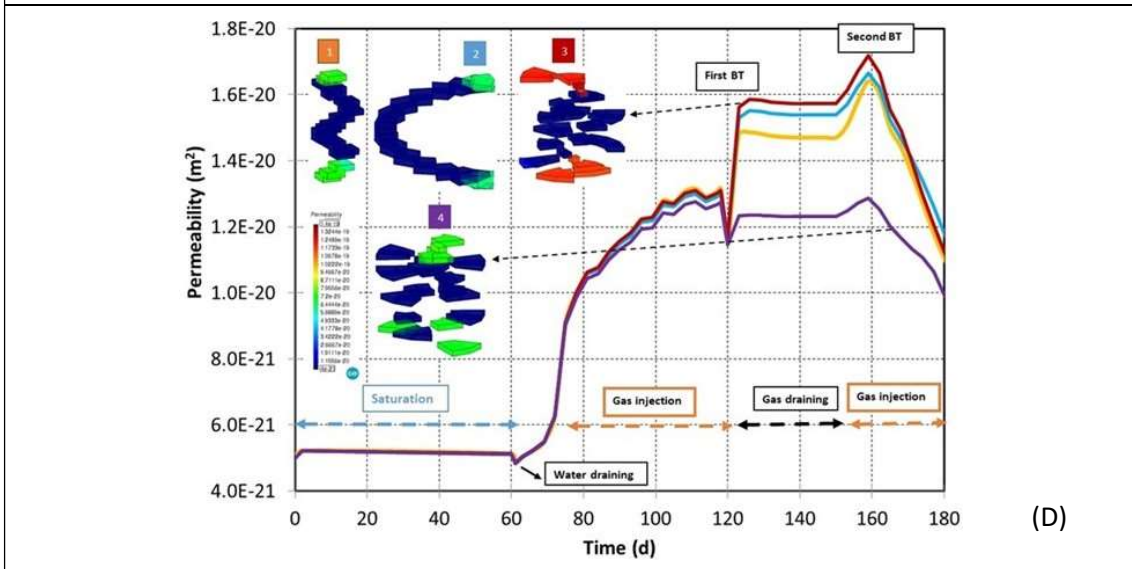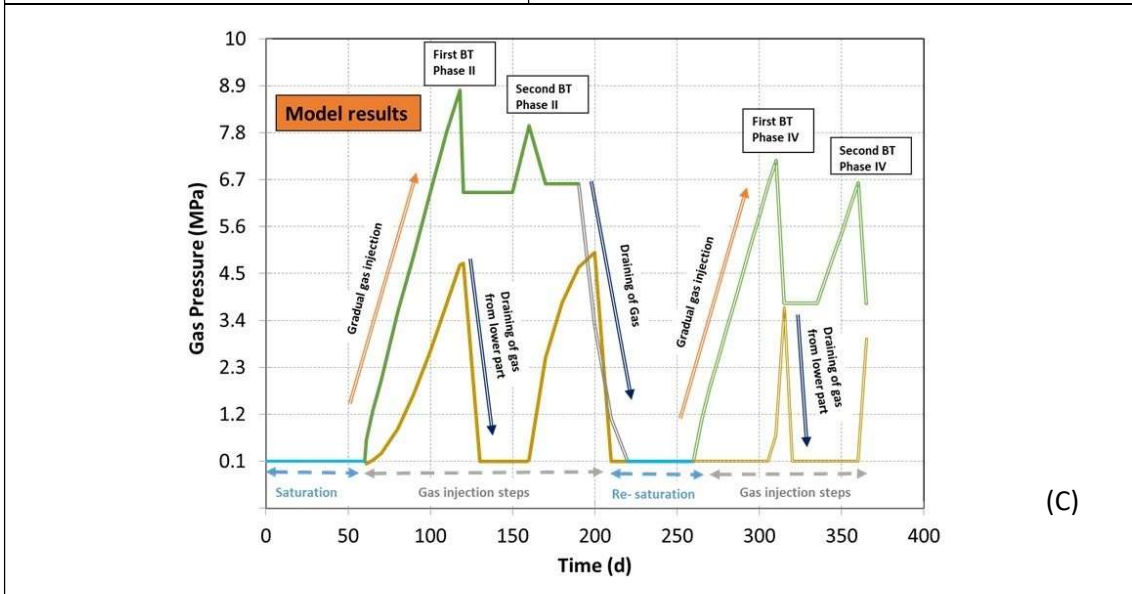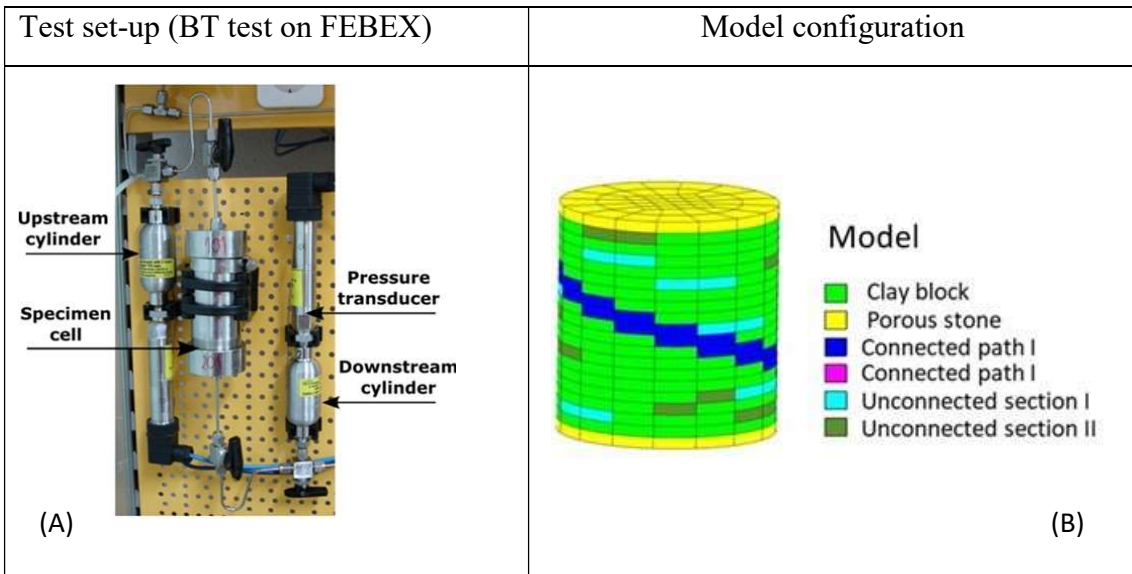
Figure 1. Test set-up (A), model configuration (B), evolution of gas pressure (C) and evolution of permeability (D).

EURAD Task 3: Hydro-mechanical modelling of PGZ Tests (COx)

To investigate gas migration into COx, Andra has followed a program of field-scale experiments. These experiments, called PGZ, has been designed to examine the migration of nitrogen in the host rock. Gas injection tests have been performed in packed off sections (intervals) of boreholes. In this document, in-situ measurements have been interpreted and compared with the model results. A summary of the tests (duration, location of the interval, borehole position, type of experiment, flow rates and achieved maximum gas pressures) is given in Table 2. In total four tests have been modelled.

A linear-elastic (considering anisotropy) model has been used in order to simulate mechanical response of COx. Cubic law for permeability (increase in permeability according gas injection) has been considered as hydraulic model. Details of hydro-mechanical model parameters can be found in [4].

Table 2. Summary of gas injection tests (PGZ into Cox).

Test	Duration	Location	Borehole position	Type of experiment	Flow rate (mLn/min)	Achieved max. gas pressure (MPa)
GAS1	420 d	Interval 2 PGZ1201	Vertical	Long term cyclic gas pressure injection test	1 to 3	9
GAS2	360 d	Interval 2 PGZ1201	Vertical or Inclined	Long term constant gas injection test	1	9.8
GAS3-A	30 h	interval 4 PGZ1002	Horizontal	Short term – gas fracturing test	500	13.01
GAS3-B	36 h	interval 4 PGZ1003	Horizontal	Short term – gas fracturing test	500	14.28

Figure 2 shows final distribution of gas pressures in each test together with comparison of measured and computed evolution of gas pressures in these four tests.

As shown in Figure 2-A, an excavated disturbed zone (EDZ) has been incorporated to the model. A 10 m box of reduced 3D geometry with different permeability zones have been used. Evolution of gas pressure during GAS1, HYDRO2 and GAS2 are shown in Figure 2-A. The model adequately reproduces the response of GAS2 but slightly overestimates some steps of GAS1.

GAS3-A consists of one step gas injection test. 13.01 MPa of maximum gas pressure has been observed in GAS3-A in 30 hours. Figure 2-B shows evolution of gas pressure of test and computed evolution of gas pressure in different models. A set of sensitivity analyses on permeability have been performed in order to optimize model response.

GAS3-B consists of two steps gas injection test and maximum pressure reaches to 14.28 MPa in 36 hours. Figure 2-B shows evolution of gas pressure of test and computed evolution of gas pressure in different models with different permeability functions.

Both GAS3-A and GAS3-B, the predicted results are in good agreement with the experimental results in certain set of model parameters defined for permeability.
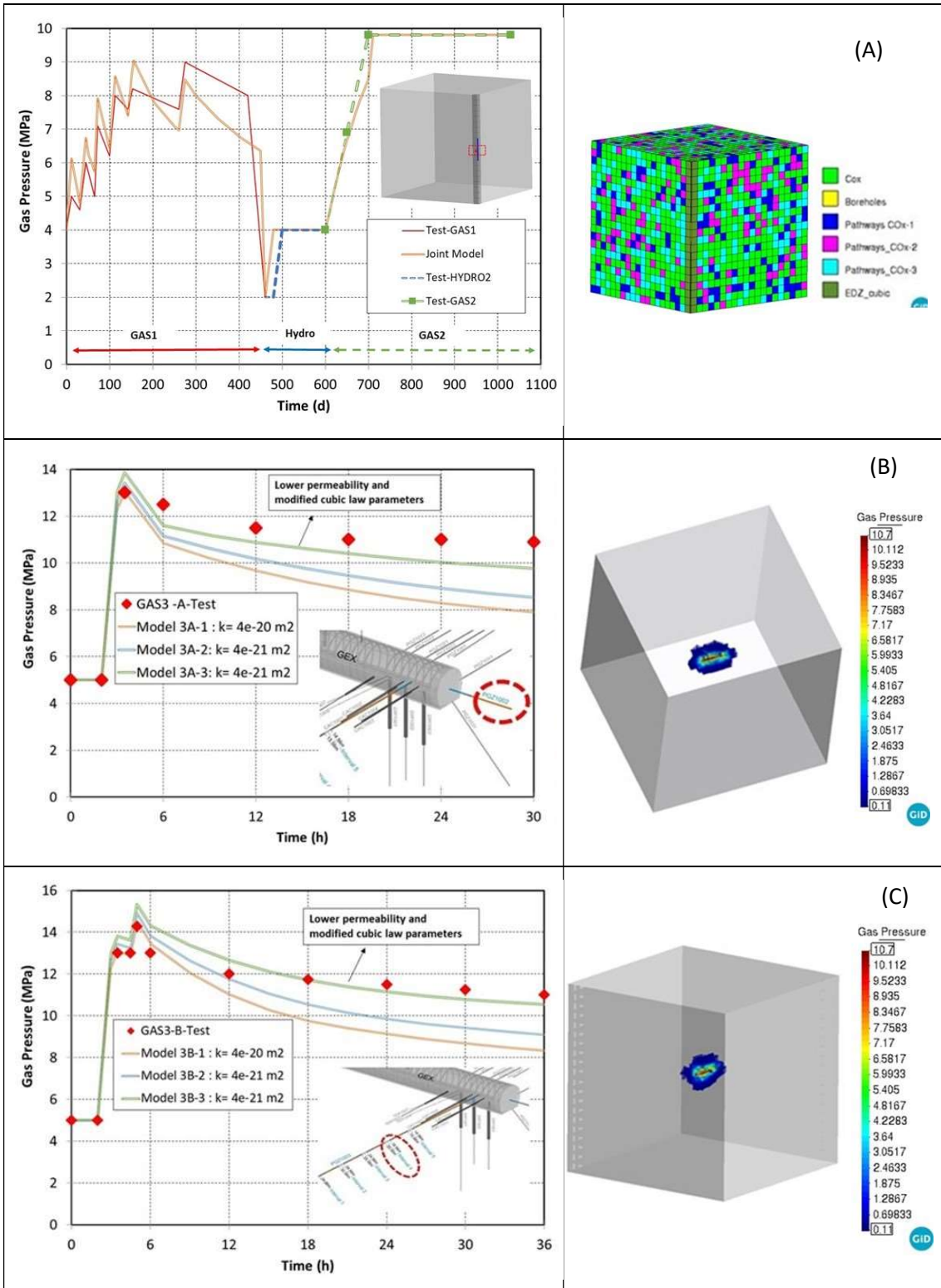
Figure 2. Final distribution of gas pressure in the models and measured and computed evolution of gas pressures in GAS1 and GAS2 (A), GAS3-A (B) and GAS3-B (C).

3 CONCLUSIONS

In the modelling of gas breakthrough (BT) tests for FEBEX (EURAD – Task 2), it has been shown the possibility of modelling of gas breakthrough test with all steps (saturation, gas injection, draining of gas, re-saturation and second gas injection) under a 3D full geometry by using complex hydro-mechanical models (cubic law for permeability and BBM as a mechanical model).

A series of long-term field scale gas injection tests (EURAD – Task 3) have been undertaken at the URL to examine the fundamental mechanisms governing the gas transport processes through Callovo-Oxfordian claystone (COx). All corresponding and available measurements from field scale gas injection tests (PGZ) on COx have been compared with the obtained numerical results. In total four in-situ field scale gas injection tests have been simulated under different 3D configurations.

REFERENCES

1. Gutiérrez Vanesa Transporte de gas en materiales de barrera, PhD dissertation, 2018

2. De La Vaissière, R., (2010) Design and Installation of the PGZ1 Experiment at Bure. FORGE Report D5.4 – VER.0

3. Toprak, E., Olivella, S. (2023) Hydro-mechanical Modelling of Gas Breakthrough Test on FEBEX. EURAD Milestone 216 and 217: Modelling progress report of tasks 2.1 and 2.2

4. Toprak, E., Olivella, S. (2022) Hydro-mechanical Modelling of PGZ Test. EURAD Milestone 124 and 125: Experimental progress report of task 3.1 / 3.2 and on modelling progress (task 3.3).

NUMERICAL ANALYSIS FOR THE SIMULATION OF CRUSHED SALT COMPACTION BEHAVIOR

Larissa Friedenberg [*], **Sebastià Olivella** [†] **and Uwe Düsterloh** [‡]

[*] Gesellschaft für Anlagen und Reaktorsicherheit (GRS) gGmbH
Repository Research Department
Theodor-Heuss-Straße 4, 38122 Braunschweig, Germany
E-Mail: larissa.friedenberg@grs.de, web page: https://www.grs.de

[†] Department of Civil and Environmental Engineering
Technical University of Catalonia (UPC)
Campus Nord UPC, 08034 Barcelona, Spain
web page: www.etcg.upc.edu/recerca/webs/code_bright/

[‡] Clausthal University of Technology[i]
Chair for Geomechanics and multiphysics Systems
Erzstraße 20, 38678 Clausthal-Zellerfeld, Germany
web page: https://www.ielf.tu-clausthal.de/fachgebiete/lehrstuhl-fuer-geomechanik-und-multiphysikalische-systeme

Key words: Crushed salt compaction, THM coupled analysis, Repository research

Abstract. *In Germany, crushed salt is considered as backfilling for open cavities in a repository in rock salt. An extensive process understanding and reliable numerical simulations for the long-term behavior are needed. This paper presents an approach for the improvement of the numerical reproduction of crushed salt compaction processes. Section 1 gives an introduction in the topic. In Section 2 the procedure is described based on an experimental program executed within the KOMPASS projects. Section 3 presents the simulation of the triaxial compaction test TUC-V2 for elaborating shortcomings. An approach based on the outcomings was developed to improve the numerical simulation and is described in Section 4.*

1 INTRODUCTION

For the deep geological disposal of high-level nuclear waste in Germany rock salt is considered as a possible host rock formation. The safety concept is based on a multi-barrier system including the backfilling of open cavities, drifts, and shafts with crushed salt. Crushed salt offers many favorable properties since it is a long-term stable material, easily available (mined-off material) and guarantees a maximum of compatibility with the host rock. With time crushed salt becomes naturally compacted by convergence which is driven through the creep ability of the rock salt. The initially high porosity of about $30 - 40\ \%$ will be reduced to an expected porosity comparable to undisturbed rock salt ($\Phi \leq 1\ \%$).

For the long-term safety assessment, a qualified prognosis of the long-term compaction behavior and the evolution of crushed salt's sealing function is needed. Therefore, it requires a fundamental process understanding, as well as a reliable numerical reproduction.

The compaction behavior of crushed salt is influenced by internal properties (e.g. grain size, grain size distribution, moisture content) and boundary conditions (e.g. temperature, stress state, strain rate), and hence involves several thermal-hydraulic-mechanical (THM)

coupled processes[iv,v]. In the current state, some uncertainties still remain in the process understanding, especially for the numerical reproduction of the crushed salt compaction process.

This paper presents an insight in an approach for improving the numerical simulation of crushed compaction using CODE_BRIGHT. Recent results on a model validation for the long-term compaction behavior of crushed salt are presented. The work is performed in parallel to the international KOMPASS projects dealing with the compaction of crushed salt for safe containment[i,iii].

2 PROCEDURE

The aim of the work is to improve the numerical simulation of the crushed salt compaction process with the idealized approach of being able to simulate different compaction tests on a uniform material with a consistent parameter set. The existing and well documented database of crushed salt was studied with the aim of carving out laboratory tests which are suitable for the numerical investigation, which means:

- Full knowledge and control about the three-dimensional stress state,
- Accurate porosity measurements,
- Including also small porosity ranges.

Some tests were found being appropriate for further numerical simulations. First, triaxial compaction tests were re-simulated for the determination of the quality of numerical reproduction and deficits in the simulation process. Then, for a fundamental validation of the constitutive model the triaxial compaction test TUC-V2 was applied which is the topic of this paper. The advantages of the TUC-V2 test are:

- The use of the KOMPASS reference material, a well-defined crushed salt material from the Sondershausen mine in Germany chosen for generic investigations[i],
- The capture of several influencing factors on the compaction behavior of crushed salt as porosity, mean stress, deviatoric stress and temperature[ii].

The TUC-V2 test in combination with more experiments executed on the KOMPASS reference material build a strong basis for the validation of the constitutive model and could lead to possible adaptions in the model formulation.

CODE_BRIGHT is used for the simulation of the crushed salt compaction process. The constitutive model is based on an additive approach of linear elastic, creep and viscoplastic strain rates:

$$d\varepsilon = d\varepsilon_{el} + d\varepsilon_c + d\varepsilon_{vp}$$ (1)

The creep part involves two components: the humidity creep represented by the fluid assisted diffusional transfer (FADT) mechanism and the creep mechanism related to the dislocation theory (DC). The viscoplastic component is involved for reproducing irreversible processes changing the structure of the granular material, like grain reorganization and sliding[vi].

3 NUMERICAL SIMULATION OF THE TEST TUC-V2

For introduction in the numerical simulation, the experimental execution of the long-term compaction test TUC-V2 is illustrated first. Afterwards, the simulation process is described followed by the evaluation of results. In the end, an approach for the improvement of the numerical simulation for crushed salt is presented.

3.1 The triaxial compaction test TUC-V2

The triaxial long-term compaction test TUC-V2 was executed by the Clausthal University of Technology (TUC) in frame of the KOMPASS projects[i,ii,iii]. The KOMPASS reference material was used for the test, contributing to a generic experimental database. Primarily, the test was planned for a duration of 150 days to investigate the isolated effect of changes in mean stress and deviatoric stress on the compaction[i]. But the test was extended and finally captures the following dependencies of compaction rate versus porosity/mean stress/temperature/deviatoric stress and volume-preserving creep versus porosity [ii].

Figure 1 shows the load history and temperature evolution for the TUC-V2 test.

3.2 Simulation of the first 150 days

Five loading stages including changes in mean stress and deviatoric stress were executed within the first 150 days of the test. For the simulation an axially symmetrical model was chosen (Figure 1b). The geometry a. The temperature effect was not considered in this phase that's why the simulation was executed HM-coupled.
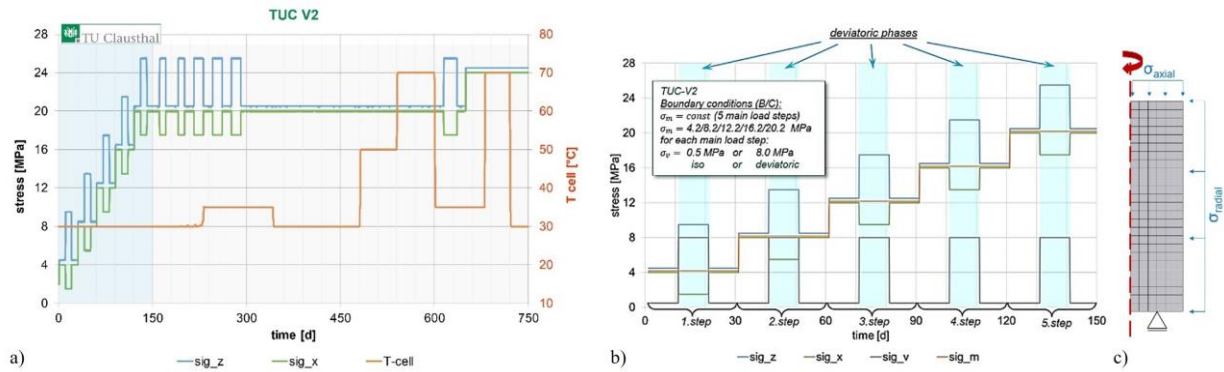
Figure 1: Triaxial compaction test TUC-V2 executed by the Clausthal University of Technology[ii]. a) Load history for the whole test. b) Load history for the first 150 days[i]. c) Numerical model.

Since no parameter set exists for the KOMPASS reference material, a first approximation was to use initial values for parameters which could not directly be received from the crushed salt material itself from another triaxial test executed on Asse mine material ("Speisesalz", As z2SP). The results using the initial parameter set (TK-031 parameter) were not satisfying and therefore, the influence of various input parameters in the constitutive equations was determined followed by a parameter improvement which leads to the final parameter set (TUC-V2 (150d)).

3.3 Evaluation of the results for the first 150 days

The numerical results for porosity evolution with time are shown in Figure 2 in comparison with the measurement data. Compaction is strongly underestimated by the TK-031 parameter set especially in the first 60 days. For the improved TUC-V2 (150d) parameter set the porosity evolution looks quite satisfying.

Additionally, the volumetric strain rates are compared in Figure 2. As indicated in the porosity results, the TK-031 parameters strongly underestimate the compaction process, hence the volumetric strain rates are about one order of magnitude too low. Up to 60 days the accordance improves for the TK-031 parameters. For the TUC-V2 (150d) parameters it is the other way round. For the first 60 days, the accordance in the strain rates is good, but is getting

worse with ongoing compaction. A detailed look into the volumetric strain rates between 90 days and 150 days shows that the slope for the rates is better for the TK-031 parameter than for the improved ones.
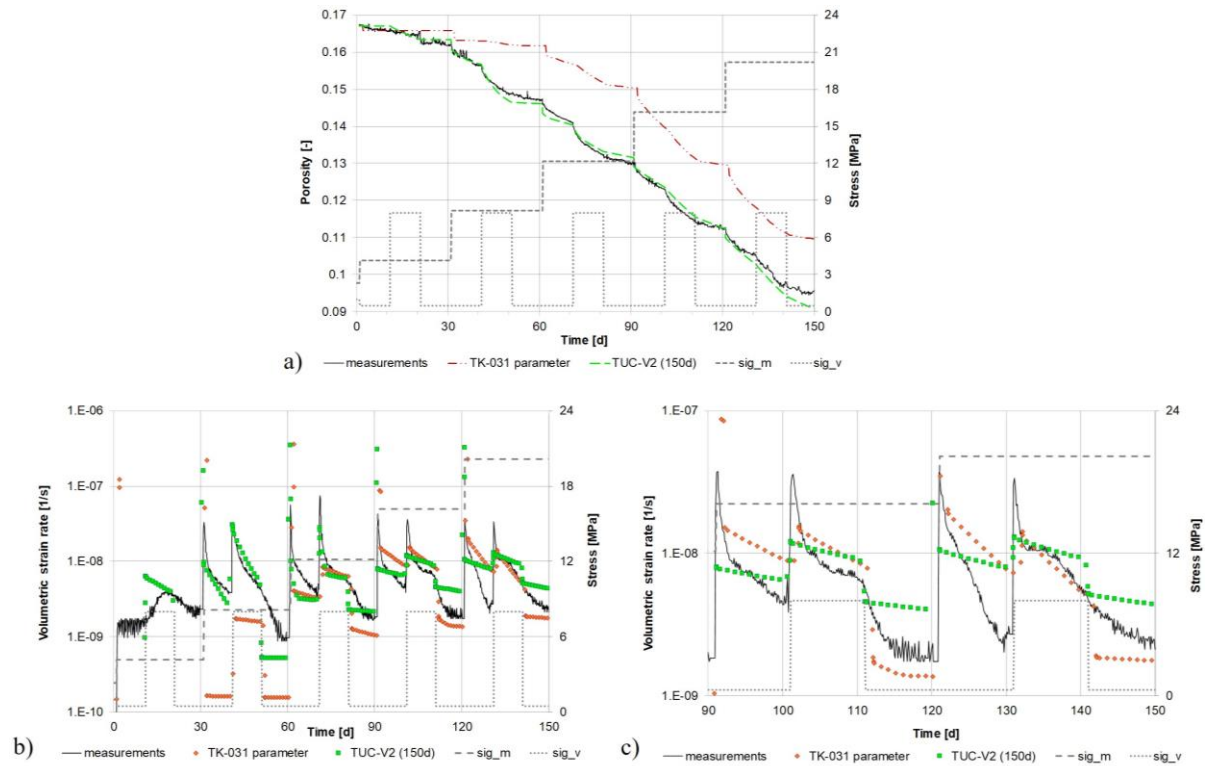
Figure 2: Results for the numerical simulation versus measurement data. a) Porosity evolution. b) volumetric strain rates. c) Detail of volumetric strain rates.

The parameter with the most influence on a successful reproduction of the porosity evolution in the TUC-V2 (150d) parameter set is pre-factor A_A in the dislocation creep law. Usually, it is derived directly from the creep class of the salt material which describes the creep ability for different salt rock types in Germany. The creep class for the KOMPASS reference material was 6 (AA = 2.08e-6), however, in this case the numerical value was not representative for simulating the compaction behavior and therefore was changed to the value corresponding to creep class 8 (AA = 1.25e-5).

The results are not satisfactory leading to the assumption that still issues exist for reproducing volumetric strain rates in a test with variations of mean and deviatoric stress.

3.4 Approach for improvement

The constitutive models for crushed salt in CODE_BRIGHT are based on an idealized geometry of grains and pores[v]. Hence geometry-based functions are implemented which are for the dislocation creep model: g^v_{DC} and g^d_{DC}, g and f. Figure 3a shows the evolution of the auxiliary functions over void ratio. The functions g^v_{DC} and g^d_{DC} are associated with volumetric and deviatoric behavior, respectively, and contain the dependence on void ratio.
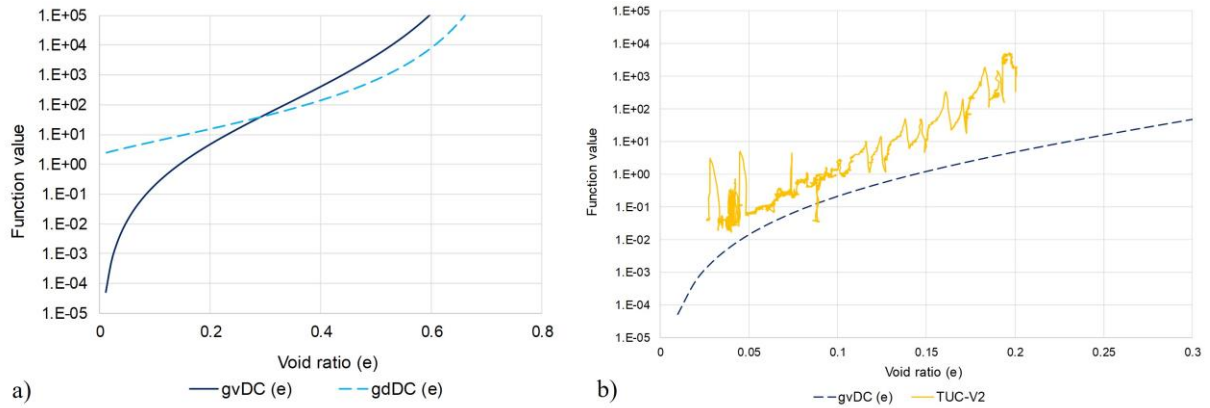
Figure 3: a) Auxiliary functions modified after Olivella and Gens (2002). b) Comparison of function g^v_{DC} as implemented in CODE_BRIGHT and as derived from the experimental data of the TUC-V2 test.

By using the experimental data from the TUC-V2 test a transformation in the geometrical function is possible. First, the focus is on the volumetric compaction behavior. Figure 3b shows the comparison of g^v_{DC} as numerical functions and as received from the experimental data of the triaxial test. The trend of both functions is different, and the correlation is not satisfying leading to the idea of giving more flexibility in the function. Therefore, two options were elaborated:

- Option 1: An old implementation is made available allowing a modification of the void ratio within the geometrical functions.
- Option 2: A new implementation of mathematical functions allowing the code user to derive the basis of the geometrical functions from the experimental data.

In the current state, both options are considered in the investigations.

Option 1 gives the possibility to modify the void ratio by calculating an equivalent void ratio following:

$$e_{equ} = e + e^3/e_0^3 * (e_{max} - e_0) \tag{2}$$

Option 2 includes the elaboration of a simple mathematical function which can be used to include the trend of the experimental data. The function is based on an exponential approach.

Figure 4a presents the volumetric geometrical functions for both options compared with the implementation and the experimental data of TUC-V2. The accordance of the improved functions with the experimental data is much better than for the current implementation. For low void ratio ranges, the Option 2 function seems to fit the function values better, however, for high void ratio ranges Option 1 might be closer to the experimental data.

The re-simulation with Option 1 was successfully done for whole test duration of TUC-V2 (Figure 4b). Since the function for Option 2 is not yet implemented in CODE_BRIGHT, a simulation was not possible to date.

The simulation with Option 1 showed a strong improvement of porosity evolution in comparison with the initially used data set. Both options promise an enhancement of numerical results for the simulation of crushed salt compaction. Option 2 is based on the experimental data as received from lab and will be followed-up.

5
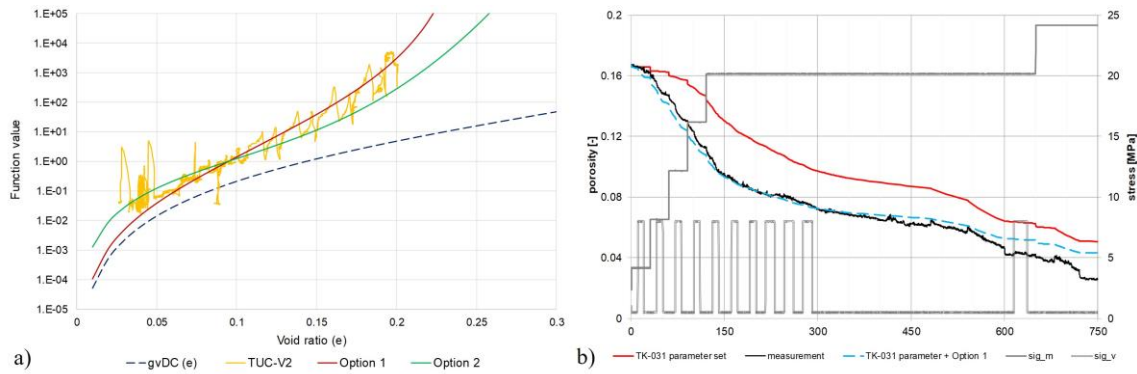
Figure 4: a) Geometrical function g^v_{DC} as implemented in CODE_BRIGHT, as derived from the test TUC-V2 and as derived from both improvement options. b) Simulation of TUC-V2 with the initial parameter set "TK-031" in comparison with the application of Option 1.

4 CONCLUSION AND OUTLOOK

The paper presents an approach for the numerical improvement of crushed salt compaction simulation. Shortcomings were identified by simulating triaxial compaction tests, especially the TUC-V2 test. The improvement approach is based on the modification of fundamental geometrical functions which are implemented on basis of an idealized geometry. Two options for the improvement were presented and for one option the success was shown.

The next step will be the implementation of mathematical functions for including Option 2 in the investigation process. Further, both options will be applied, compared, and validated.

REFERENCES

[i]   Czaikowski, O., Friedenberg, L., Wieczorek, K., Müller-Hoeppe, N., Lerch, C., Eickemeier, R., Laurich, B., Liu, W., Stührenberg, D., Svensson, J. K., Zemke, K., Lüdeling, C., Popp, T., Bean, J., Mills, M., Reedlunn, B., Düsterloh, U., Lerche, S., Zhao, J. 2020. Kompass: Compaction of crushed salt for the safe containment (GRS-). Köln, Garching b. München, Berlin, Braunschweig. Gesellschaft für Anlagen- und Reaktorsicherheit (GRS) gGmbH.

[ii]   Düsterloh, U., Lerche, S., Saruulbayar, N. 2022. Crushed salt compaction - a new approach for lab test analysis, physical modelling and numerical simulation: Part 1: Development and validation. In S. Hangx, A. R. Niemeijer, J. de Bresser, C. J. Spiers, M. R. Drury, M. Gazzani, & P. A. Fokker (Eds.), The Mechanical Behavior of Salt X: Proceedings of the 10th Conference on the Mechanical Behvaior of Salt (SaltMech X), Utrecht, The Netherlands, 06 - 08 July 2022. CRC Press

[iii] Friedenberg, L., Bartol, J., Bean, J., Czaikowski, O., Düsterloh, U., Gartzke, A.-K., Hangx, S., Laurich, B., Lerch, C., Lerche, S., Lippmann-Pipke, J., Liu, W., Lüdeling, C., Mills, M. M., Müller-Hoeppe, N., Popp, T., Rabbel, O., Rahmig, M., Reedlunn, B., . . . Zhao, J. 2022. Compaction of crushed salt for the safe containment - Overview of phase 2 of the KOMPASS project. In S. Hangx, A. R. Niemeijer, J. de Bresser, C. J. Spiers, M. R. Drury, M., Gazzani, & P. A. Fokker (Eds.), The Mechanical Behavior of Salt X: Proceedings of the 10th Conference on the Mechanical Behvaior of Salt (SaltMech X), Utrecht, The Netherlands, 06 - 08 July 2022 (pp. 283–291). CRC Press.

[iv]   Hansen, F. D., Popp, T., Wieczorek, K., Stührenberg, D. 2014. Granular Salt Summary: Granular Salt Summary: Reconsolidation Principles and Applications: Fuel Cycle Research & Development. Sandia National Laboratories.

[v]   Olivella, S., Gens, A. 2002. A constitutive model for crushed salt. International Journal for Numerical and Analytical Methods in Geomechanics, 26(7), 719–746. https://doi.org/10.1002/nag.220

PERFORMANCE OF BOOM CLAY SUBJECT TO THERMAL LOADING: APPLICATION TO THE PRACLAY IN-SITU EXPERIMENT

Fei Song [*], Antonio Gens [†]

[*] Universitat Politècnica de Catalunya (UPC), Campus Nord UPC, 08034 Barcelona, Spain
E-mail: fei.song@upc.edu

[†] Universitat Politècnica de Catalunya (UPC) – CIMNE, Campus Nord UPC, 08034 Barcelona, Spain
E-mail: antonio.gens@upc.edu

Keywords: THM modelling, Boom Clay, PRACLAY heating test, Strain localization

Abstract. *In this study, the coupled Thermo-Hydro-Mechanical (THM) modelling has been carried out for a full-scale PRACLAY heating test. In the numerical simulations, an advanced elastoplastic model with damage and nonlocal formulation is used to represent the behaviour of Boom Clay, whereas a bi-linear model is adopted to simulate over-excavation. The evolution of the damage zone due to underground excavation and thermal pressurization have been identified. Experimental data in terms of temperature and pore pressure in the past twenty years are available. A good agreement is observed between numerical and experimental results. The current research provides a deeper insight into the coupled THM behaviour of high-level radioactive disposal facilities subjected to thermal loading.*

1 INTRODUCTION

Geological disposal is widely recognized as the most feasible and effective solution for High-level Nuclear Waste (HLW) and Spent Fuel (SF) disposal [i]. In the implementation of HLW disposal, underground excavation of the galleries leads to stress redistribution around the gallery and, therefore results in the evolution of an excavation damage zone [ii]. Additionally, after storing the nuclear waste package, temperature increases in the host rock, resulting in a pore pressure rise due to thermal pressurization. In conclusion, the performance of HLW disposal must be analysed in a coupled Thermo-Hydro-Mechanical (THM) framework.

In this study, the large-scale PRACLAY heater test, performed in the HADES (High-Activity Disposal Experimental Site) URL (Underground Research Laboratory) will be analysed. In section 2, the in-situ experiment of the PRACLAY heating test will be introduced. Section 3 will explain the adopted THM formulations. Sections 4 and 5 will describe the numerical model and obtained numerical results. Numerical predictions will be compared with experimental data to validate the adopted numerical approaches. In addition, strain localization will be identified in the numerical analyses.

2 PRACLAY IN-SITU EXPERIMENT

The large-scale PRACLAY Heater test is being carried out in the HADES URL in Mol (Belgium) [iii]. From 04-Oct-2007 to 06-Nov-2007, the PRACLAY gallery was constructed in Boom Clay, perpendicular to the existing connecting gallery. The PRACLAY gallery is 45 m long with an external diameter of 2.5 m and the gallery is supported by concrete lining rings

with a thickness of 0.3 m and a length of 0.5 m. Most of the rings have a concrete grade of C80/95.

From January to May 2012, a total liquid volume of about 43 m^2 was injected into the gallery and the pore water pressure was increased artificially in five steps, as shown in Figure 1 (a). The hydration of the backfilled gallery was then completed by the water flowing from the surrounding Boom Clay into the gallery. At the moment of starting the heating test (03-Nov-2014), the pore pressure achieved 1 MPa. During the heating stage of the experiment, an undrained boundary condition was considered at the gallery wall. The heater power was stepwise increased until the temperature at the lining extrados reached 80 °C, as shown in Figure 1 (b).

A large instrumentation network with about 1100 sensors was set up around the PRACLAY gallery to monitor the response of Boom Clay from the gallery excavation till the end of the heater test [iii]. In-situ experimental results are presented in Section 5, which will be used to compare with numerical predictions.
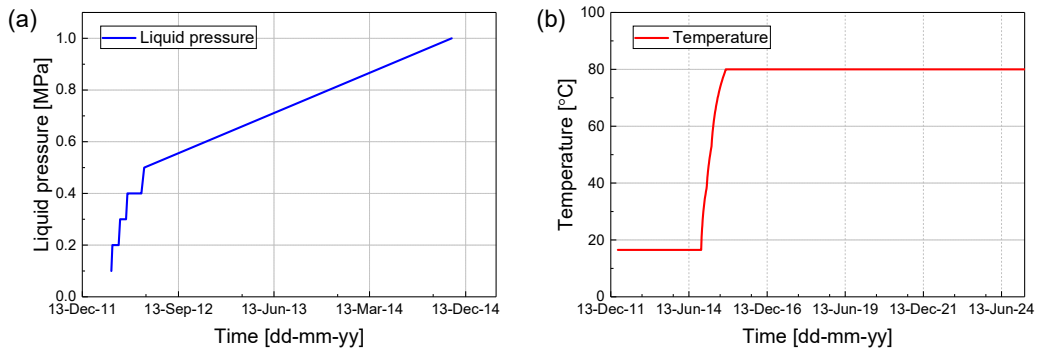
Figure 1: (a) Pore pressure boundary condition at the inner boundary of concrete lining in the artificial injection stage, and (b) Temperature boundary condition at the lining extrados.

3   THM FORMULATIONS

In the application of HLW disposals, the behaviour of argillaceous rocks subjected to thermal loading has to be considered in a coupled THM framework [iv]. Temperature variations can influence hydraulic behaviour because of temperature-dependent fluid viscosity and thermal pressurization changes in pore water pressure. Meanwhile, thermal-induced strains can be developed due to temperature variations and, thermal-mechanical coupling occurs. At the same time, hydraulic and mechanical behaviour are coupled with each other: changes in hydraulic conditions influence mechanical behaviour by changing the pore pressure and effective stresses, while changes in strains impact liquid pressure and damage-induced permeability. Heat convection is a potential effect of hydraulic behaviour on the temperature field but it is generally negligible in a low permeability medium.

In the research presented, an elastoplastic constitutive model with damage and nonlocal formulation is used to represent the mechanical properties of Boom Clay. The advanced elastoplastic constitutive model has been implemented in the computer code Code_Bright based on a coupled THM formulation founded on a macroscopic approach. Code_Bright was developed in the context of the continuum theory for porous media. In this study, the coupled THM formulations for saturated porous media will be analysed, considering two phases (solid and liquid) and two species (mineral and water). The formulation incorporates basic thermal, hydraulic and mechanical phenomena in a coupled manner and involves the simultaneous solution of seceral fundamental balance equations: solid mass, water mass, momentum

(equilibrium) and energy. A more detailed description of the finite element formulation utilized in Code_Bright can be found in Olivella et al. [v].

4 NUMERICAL MODEL

4.1 Geometry and initial conditions

The model is representative of the mid-plane of the PRACLAY Heater test (around Ring 50). Only a quarter of the cross-section is considered due to the symmetric nature of the problem. The calculatopn domain measures 100 m in the x- and y- directions. An over-excavation of 6 cm is assumed and the excavation radius is estimated to be 1.31m. The inner and outer radii of the concrete lining are 0.95 m and 1.25 m, respectively.

The initial temperature and pore pressure in the Boom clay are 16.5 °C and 2.25 MPa, respectively. The initial horizontal and vertical total stresses in the Boom clay are 3.825 MPa and 4.5 MPa, respectively. Constant initial pore pressure (0.1 MPa) and stresses (0.1 MPa in all directions) are assumed in the concrete lining.

4.2 Modelling stages and boundary conditions

As shown in Figure 2, four different modelling stages have been considered in the current numerical simulations.
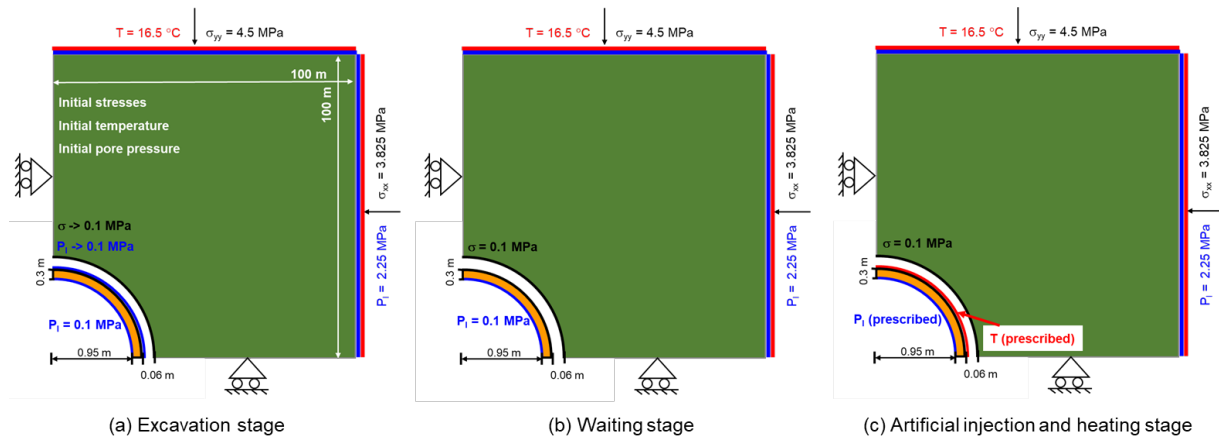
Figure 2: Boundary conditions at different modelling stages: (a) The excavation stage, (b) The waiting stage, and (c) The artificial injection and heating stage.

In each modelling stage, the boundary conditions are applied as follows:

- **The excavation stage** (from 04-Oct-2007 to 06-Nov-2007). The smoothed excavation method [vi] is used to simulate the excavation process with the stresses inside the excavated elements are linearly reduced from the initial stresses to 0.1 MPa. During excavation, the host rock freely deforms until contacting the outer boundary of the concrete lining; after that, the host rock and the concrete lining deform together, and support forces will be provided by the interaction between the host rocks and the concrete lining. The pore pressure at the gallery decreases from 2.25 MPa to atmospheric pressure (0.1 MPa).
- **The waiting stage** (from 06-Nov-2007 to 05-Mar-2012). The pore pressure in the inner boundary of the concrete lining is maintained at 0.1 MPa.
- **The artificial injection stage** (from 05-Mar-2012 to 13-Nov-2014). The pore pressure is prescribed at the inner boundary of the concrete lining according to Figure 1 (a).

- **The heating stage** (from 03-Nov-2014). An undrained hydraulic boundary condition is applied to the concrete lining. Based on the measured temperature at the lining extrados, a temperature boundary condition is set at the lining extrados, as shown in Figure 1 (b). The heater was switched on 03-Nov-2014, and the temperature at the lining extrados reached 80 °C on 17-Aug-2015; a constant temperature of 80 °C will be maintained at the lining extrados for 10 years till 17-Aug-2025.

4.3 Constitutive models

An elastoplastic model is used for Boom Clay, with the consideration of hardening-softening, anisotropy of stiffness and strengths (see Figure 3a), hyperbolic approximation to the Mohr-Coulomb yield surface, non-associated flow rule and nonlocal formulation (see Figure 3b). More detailed information about the utilized elastoplastic constitutive model can be found in Manica [vii]. An elastic constitutive model is adopted to represent the properties of concrete lining.

In addition, a bi-linear element is used to simulate the behaviour of air gap elements, as shown in Figure 3(c). Two different values of Young's moduli are used: one for the open gap with a very small value and the other one for the closed gap with a much larger value [viii]. The threshold between the open and closed gaps is controlled by the value of volumetric strain.
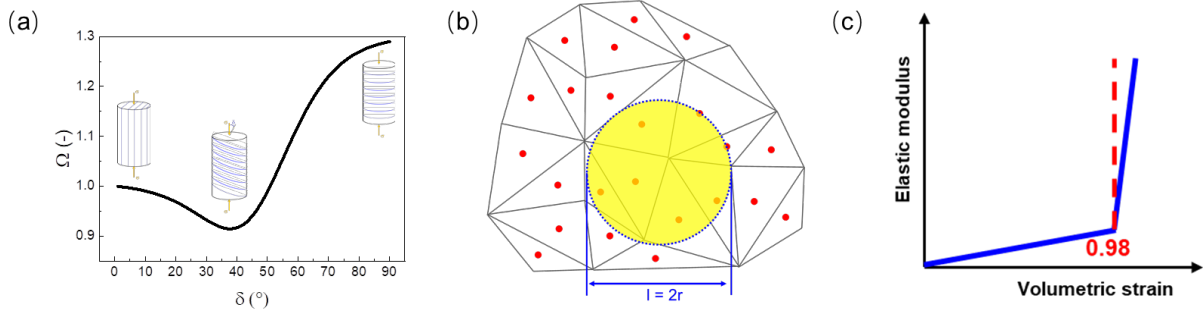
Figure 3: (a) Anisotropy of strength, (b) Adopted nonlocal approach in the adopted elastoplastic constitutive model, and (c) Bi-linear model for the air gap element.

5 NUMERICAL PREDICTIONS OF THE IN-SITU EXPERIMENTAL DATA

Figure 4 shows the comparisons of temperature and pore water pressure between numerical predictions and experimental data. A good agreement can be observed, validating the utilized numerical approaches and the obtained numerical results. In Figures 4-5, it can be observed that, in the artificial injection stage, pore pressure increases due to the injection of liquid. Furthermore, in the heating stage, an undrained boundary condition is applied at the gallery wall and the pore pressure increase due to the thermal pressurization. Thermal pressurization is caused by the difference in thermal expansion coefficients between the solid skeleton and the pore water [ix].

To make further investigation of THM responses of the Boom Clay, Figure 5 shows the contours of pore pressure and plastic shear strains in the vicinity of the gallery. At the beginning of the artificial injection (05-Mar-2012), shear bands developed around the gallery due to underground excavation. In addition, in the artificial injection and heating stages, the evolution of pore pressure contributes to the further development of plastic shear strains.
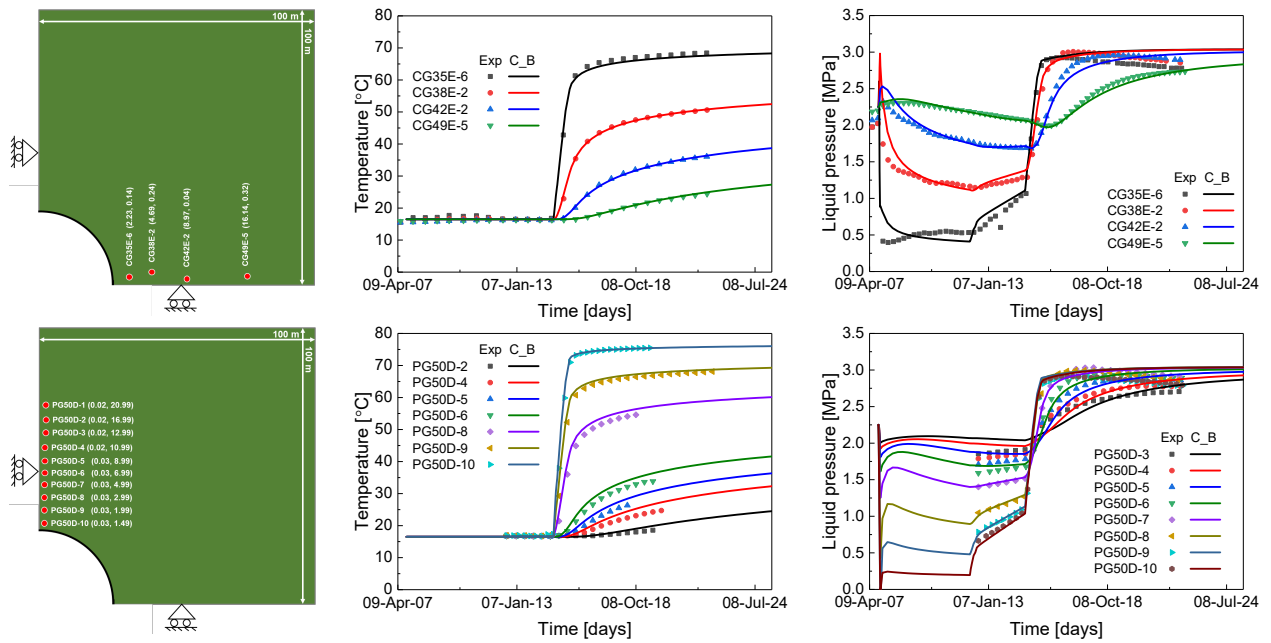
Figure 4: Comparison of temperature and pore pressure between numerical and experimental results.
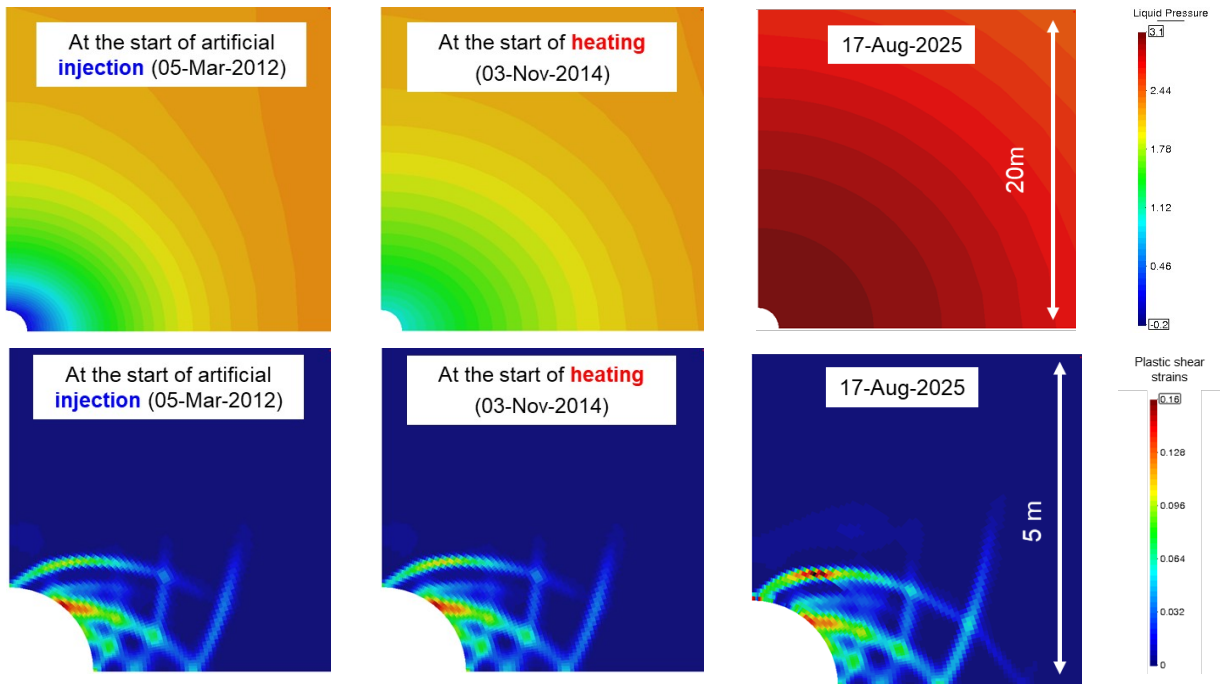
Figure 5: Contours of pore water pressure and plastic shear strains in the vicinity of the gallery.

6 CONCLUSIONS

In this study, numerical simulations have been performed to analyse the large-scale PRACLAY Heater test. In the numerical analyses, an advanced Hyperbolic Mohr-Coulomb elastoplastic model with damage and nonlocal formulation has been used to represent the behaviours of Boom Clay. In addition, a bi-linear model is used to simulate the properties of air gap elements. Experimental data in the past twenty years has been used to validate

numerical results. A good agreement has been observed between numerical and experimental results, in terms of both temperature and pore pressure. In addition, the evolutions of pore water pressure and damage zone subjected to underground excavation and thermal pressurization have been identified.

ACKNOWLEDGEMENTS

REFERENCES

[i]   Gens A, Barboza de Vasconcelos R, Olivella S (2020) Towards higher temperatures in nuclear waste repositories. In: E3S Web of Conferences. EDP Sciences, pp 1–8

[ii]   Mánica M, Gens A, Vaunat J, et al (2021) Numerical simulation of underground excavations in an indurated clay using non-local regularisation. Part 1: Formulation and base case. Géotechnique 1–21.

[iii]   Villar, M.V., Armand, G., Conil, N., et al (2020). D7.1 HITEC. Initial State-of-the-Art on THM behaviour of i) Buffer claymaterials and of ii) Host clay materials. Deliverable D7.1 HITEC. EURAD Project, Horizon 2020 No847593.

[iv]   Song F, Collico S, Gens A (2022) Coupled THM responses of callovo-oxfordian claystone subject to thermal loading. In: 2022 Workshop of CODE_BRIGHT USERS. Barcelona, Spain

[v]   Olivella S, Gens A, Carrera J, Alonso EE (1996) Numerical formulation for a simulator (CODE_BRIGHT) for the coupled analysis of saline media. Eng Comput (Swansea, Wales) 13:87–112.

[vi]   Song F, Rodriguez-Dono A, Olivella S (2021) Hydro-mechanical modelling and analysis of multi-stage tunnel excavations using a smoothed excavation method. Comput Geotech 135:104150.

[vii]   Mánica M (2018) Analysis of underground excavations in argillaceous hard soils - weak rocks. Ph.D. thesis, Universitat Politècnica de Catalunya (UPC).

[viii] Tourchi S, Vaunat J, Gens A, et al (2021) A full-scale in situ heating test in Callovo-Oxfordian claystone: observations, analysis and interpretation. Comput Geotech 133:104045.

[ix]   Vu MN, Armand G, Plua C (2020) Thermal Pressurization Coefficient of Anisotropic Elastic Porous Media. Rock Mech Rock Eng 53:2027–2031.

MODELLING SOIL-VEGETATION-ATMOSPHERE IN A FIELD EXPERIMENT

Ehsan Badakhshan and Jean Vaunat

Department of Civil and Environmental Engineering
Technical University of Catalonia (UPC)
Campus Nord UPC, 08034 Barcelona, Spain

Key words: Soil-atmosphere-vegetation interaction, Slope, Water retention curve.

Abstract. *In this paper, a soil-atmosphere-vegetation interaction, comprised of the state of the atmosphere and its interactions with vegetation in terms of precipitation, wind, temperature, and radiation, is used based on a Finite Element code (CODE_BRIGHT) to predict the slope response to atmospheric actions. For this aim, an atmospheric boundary condition as a flux is applied on the surface of the simulated slope to impose meteorological data that vary in time. At the root zone, a surface flux is applied to interact with the atmosphere flux boundary condition. For the validation purpose, the data from an instrumented slope in Barcelona is utilized. The response of slope to rainfall infiltration and its interaction with the atmosphere demonstrated that vegetation plays a serious role in thermo-hydraulic variables.*

1 INTRODUCTION

Slope mass movement triggered by erosion in presence of temperature changes and other phenomena related to climatic actions like frequent periods of torrential rainfall and drought has become one of the most serious environmental disasters [1,2]. A clear example is the natural hazards caused on slopes or natural hillsides due to heavy rainfall and temperature changes that cause wetting and drying conditions in soils [2].

The evaluation of the soil-atmosphere-vegetation interaction effect on slopes has been recognized as one of the main induced factors of slope mass movement. Destabilizing factors such as desiccation cracking (drying) and infiltration process (wetting) in repetitive cycles induced by climate change alter the mechanical and hydraulic properties and creates planes of weakness, and change the pore water pressure of the soil. Forecasting of such phenomena, adequate knowledge of the changes in hydrogeological conditions under climatic agents is needed [3].

In this research, the Code_Bright, a finite element model, improved in considering the hysteretic behavior of soil water retention curve, is used to simulate the infiltration, water and heat exchange between the soil and the atmosphere, and vegetation interactions in response to meteorological forces. Furthermore, it is discussed how the soil-atmosphere-vegetation interaction affects the behavior of slopes covered by vegetation.

2 SOIL-VEGETATION-ATMOSPHERE INTERACTION

The vegetation interactions contain exchanges in heat through the fraction of the solar radiation reaching the surface of the soil and fluid mass. In vegetation, the water dominantly loses by stomata, which are small holes in the leaf of plants through which water vapor and gases pass. In this case, the role of vegetation covers in terms of transpiration (i.e., uptake and

vaporization of water through plant tissues), and heat exchanges should be applied at the upper part of the soil layer. Therefore, considering the effect of vegetation on the slope's response, a flux model is utilized to simulate the water infiltration into and out of the root zone. This flux exerts vegetation's data as inputs, then computes the transpiration, evaporation, drainage from the root zone, and water interception through the vegetation. For this aim, in the root zone, a mass balance equation should be solved. Therefore, the soil-water balance will be computed for the root zone, as is shown in Figure 1. The model input data are the meteorological data: solar radiation (R_{si}), precipitation (P), air temperature (T_a), relative humidity (h_r), wind speed (u_a) and runoff (R_{off}), the soil thermo-hydro characteristics and the vegetation canopy parameters. The hydraulic and the thermal boundary conditions are calculated from meteorological data of the actual time step and the soil thermo-hydro state corresponding to the previous time step.
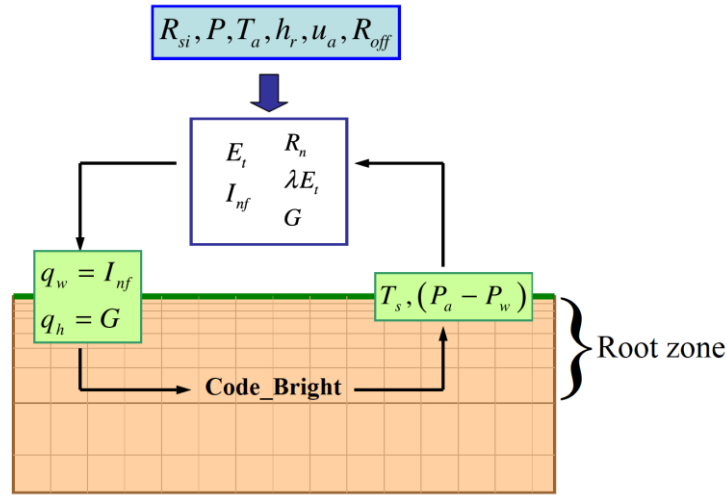
Figure 1: Schematic view of Mass balance and energy balance on soil-vegetation-atmosphere interface.

According to Sellers et al. [4], the evapotranspiration flux is defined by the resistances for both plant and soil, which define the sensible and latent heat. At the soil surface, two types of vegetation systems (grass cover and canopy) parallelly function along with the ground evaporation. The grass system is defined by several flow movement resistances in series positions as r_{sf} (soil/plant), r_{pf} (plant), and r_{af} (plant/atmosphere). These resistances control the flux of transpiration between groundwater potential at the plant root level and water potential at the plant leaf level. In a similar way, the system of canopy contains resistances of r_{sc} (soil/canopy), r_{pc} (canopy), and r_{ac} (canopy/atmosphere). Based on this system, the flux of evaporation based on the difference between the concentration of vapor at the leaf and the air is as follow

$$E_v = (1 - veg)\frac{1}{r_a}(\rho_{va} - \rho_v)$$
(1)

where r_a is the aerodynamic resistance (the atmosphere resistance on top of the leaf), and other parameters are defined before. Furthermore, veg is the vegetized surface per unit area of ground (vegetation fraction), which is computed as the vertical projection of vegetation to the ground surface. The flux of transpiration at the canopy level is expressed as the difference between vapor density at the atmosphere and leaf levels. Since the relative humidity inside the leaf is almost 100%, it stands as the vapor density at saturated conditions, which is associated

only with the leaf temperature as

$$E_T = veg \frac{1}{r_a + r_s} \left(\rho_{vasat} - \rho_{va} \right) \qquad (2)$$

where r_s is the leaf surface resistance by the stomata and ρ_{vasat} is the saturated atmosphere's absolute humidity. In this case, the r_s and r_a act in series. Hence, the flux of water j_a^w will be the sum of evaporation (E), rainfall (P), the advective flux of vapor of gas phase (j_g^w), and the surface runoff (j_{sr}) as follow.

$$j_a^w = P + E + j_g^w + j_{sr} \qquad (3)$$

3 SLOPE SIMULATIONS AND VERIFICATIONS

The defined model is examined by the Code_Bright for carrying out the numerical computation and verifying the validity of the model. Figure 2 shows the constructed slope at Parc UPC of Barcelona, Spain, which is selected for the model verification [2]. The slope is 18 m in length, 12 m in width, and 2.5 m in height with a slope angle of 32°. It is contained silty sand materials and is covered at 0.56 m depth by an impervious polyethylene geomembrane to avoid infiltration of water to other parts of the slope. To simulate the slope, each side is extended by 15 meters in length and 15 meters in the depth to reduce the effects of the boundaries on the model results. For the simulations, the initial conditions were a 5°C temperature, and constant gas and liquid pressure as 0.1 MPa. Also, the time-varying atmospheric data such as atmospheric temperature, atmospheric gas pressure, relative humidity, radiation, cloud index, rainfall, wind velocity, longwave radiation, and atmospheric transmissivity are considered from the field-measured meteorological data.

Figure 2: The north face of constructed slope in Barcelona.

4 RESULTS AND DISCUSSIONS

The capability of the used model for describing the thermo-hydro simulation of slopes is investigated by comparing the numerical results with measurement data. The following sections analyze the variation in soil temperature (T) at different depths of the slope. Also, the results of simulations are compared with the measurement data. To simulate the slope, each side is extended by 15 meters in length and 15 meters in the depth to reduce the effects of the boundaries on the model results. To carry out the modeling, the finite element mesh structured

with 851 quadrilaterals and 796 nodes is defined, carrying out a concentration of elements from the superficial part to the internal part of the slopes in order to obtain more detailed and precise results in the area where soil-atmosphere interaction occurs as indicated in Figure 3. Also, since in focus of this study is the behavior of slope under atmospheric conditions, the porosity is considered as a constant and the soil as a non-deformable.

For the simulations, the initial conditions were a 5°C temperature, and constant gas and liquid pressure of 0.1 MPa. Also, the time-varying atmospheric data such as atmospheric temperature, atmospheric gas pressure, relative humidity, radiation, cloud index, rainfall, wind velocity, longwave radiation, and atmospheric transmissivity are considered from the field-measured meteorological data. The soil input parameters which are utilized for the models are listed in Table 1.
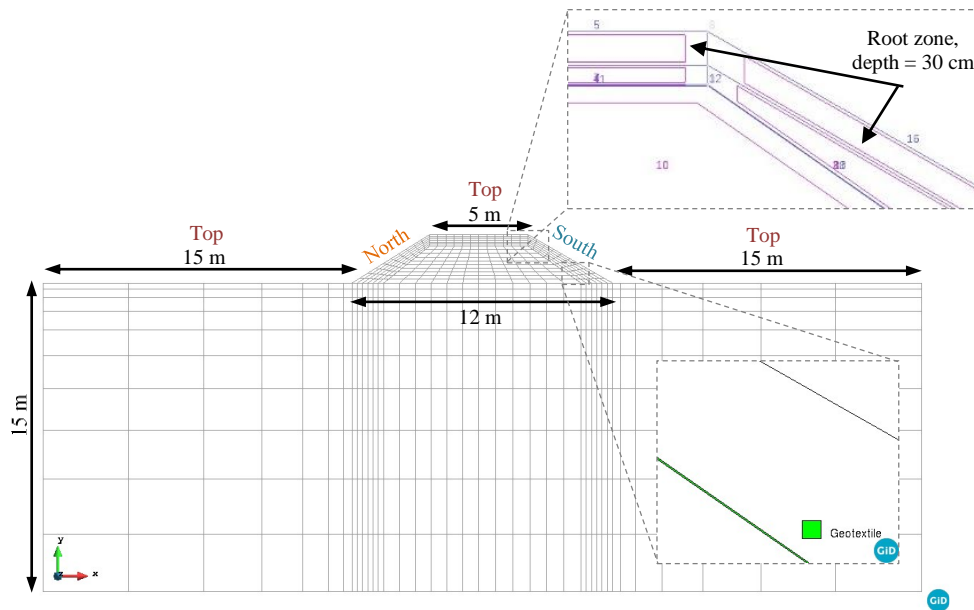
Figure 3: The generated mesh of the modeled slope.

4.1 Temperature analysis

In Figure 4, the soil temperature of slope at different depths for both north and south sides are compared with the measurement data from the field. The predictions for the temperature in different depths are fairly consistent with the recorded data by sensors. Also, based on this figure, it is clear that under the same environmental conditions, the soil temperature on the north and south slope profiles is different. The difference in soil temperatures is due to the amount of radiation received by each slope.

The southern slope, receiving directly a greater amount of radiation, presents higher temperatures with greater oscillation, especially in the shallow depth. The surface temperature on each slope makes it possible to visualize the difference and fluctuations in temperature that exist. There is a 15°C difference between the maximum temperatures recorded every 5 minutes and about 1.7°C between minimum temperatures. For a greater depth of 36 cm, the maximum difference is 2.2°C and the minimum is 4.5°C. At this depth on both slopes, the oscillations are smaller. The daily oscillations practically disappear at a depth of 36 cm. These differences have a strong effect on the amount of heat available in the soil to allow for water phase changes associated to evaporation.

Property	Slope		Geomembrane	
Porosity, ϕ	0.3		0.1	
Intrinsic permeability (m^2)	8.5e-16		1e-20	
Liq. phase rel. permeability, λ	0.3		0.3	
Water retention curve				
Type	Hysteretic model		van Genuchten model	
	P_{0d}	0.6	P_0	2.27
	σ_0	0	σ_0	0.072
	m	0.5	m	0.8
	$S_{lr}\xi$	0.0105	S_{lr}	0.034
	S_{ls}	1	S_{ls}	0.913
	P_{0w}	0.017	-	-
	γ_d	1.20	-	-
	s_0	0.013	-	-
	S_{l0}	0.269	-	-
	γ_w	0.43	-	-

Table 1: Input parameters for the simulation of the slopes.
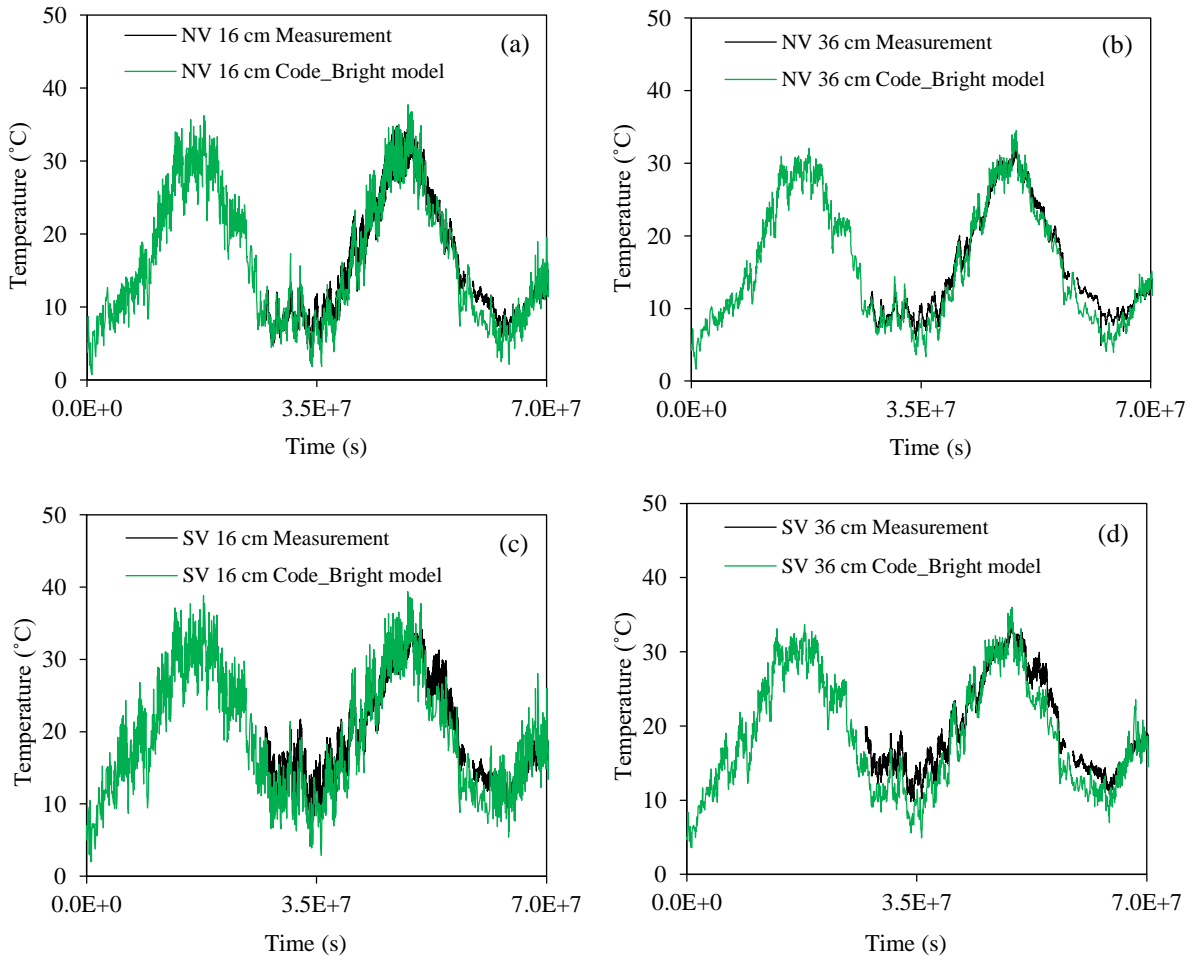
Figure 4: Comparison of soil temperature of the numerical results with the field measurement data for different depths in vegetated slope at north side, a)16 cm, b) 36 cm, and south side, c) 16 cm, and h) 36 cm.

4.2 Volumetric water content analysis

The evolution of the volumetric water content (VWC) is presented in Figure 5, which corresponds to calculated data and those recorded by the sensors on each slope. Also, to make a better comparison among volumetric water content changes and rainfall, the recorded precipitation at the field weather station is added to this graph. This figure also shows the difference between using the hysteretic SWRC and non-hysteretic SWRC. The results obtained with the Code_Bright in hysteretic SWRC conditions, provide a relatively similar trend to what is recorded with the sensors. In periods corresponding to rainfall, the slope experiences wetting processes that appear in the graphs as a sudden change (peaks) in the continuity of the results, especially when the soil has a low VWC.
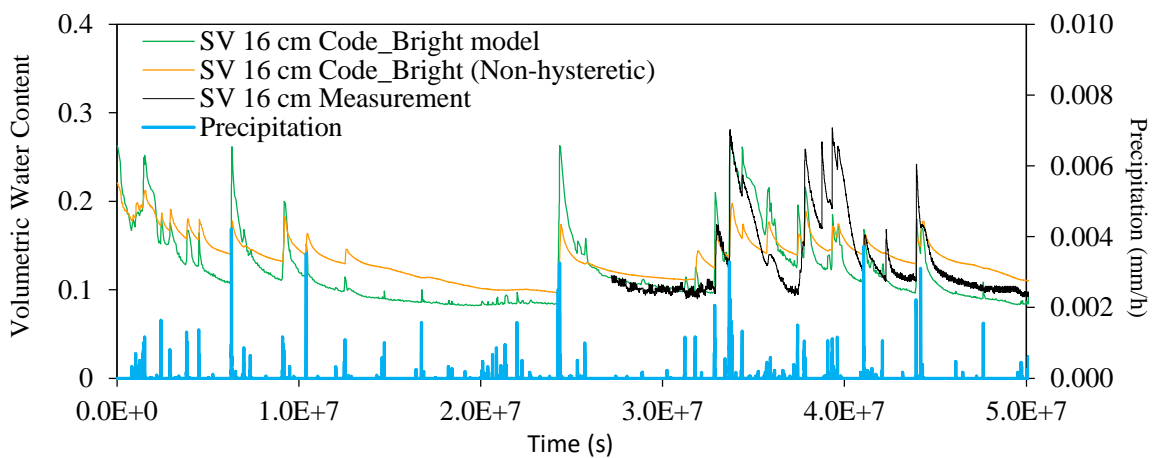
Figure 5: Comparison of the results of volumetric water content with measurement data for vegetated slope in both non-hysteretic and hysteretic conditions.

5 CONCLUSIONS

The soil-atmosphere-vegetation interaction simulations of slopes have been carried out using the numerical model of finite elements for coupling the Thermo-Hydraulic processes. From this research, it is concluded that the modeling carried out in this study is fundamentally satisfactory. It has been possible to reproduce the patterns of behavior of the vegetated slopes based on the environmental boundary conditions, vegetation flux and the properties of the soil, such as the hysteretic soil water retention curve, which is compatible with the type of soil used in the construction of the slope.

REFERENCES

[1] Casini, F., Vaunat, J., Romero, E., Desideri, A., 2012. Consequences on water retention properties of double-porosity features in a compacted silt. *Acta Geotechnica*, 7 (2), 139–50.
[2] Oorthuis, R., Vaunat, J., Hürlimann, M., Lloret, A., Moya, J., PuigPolo, C., Fraccica, A., 2021. Slope orientation and vegetation effects on soil thermo-hydraulic behavior. An experimental study. *Sustainability*, 13, 1–14.
[3] Gens, A., 2010. Soil–environment interactions in geotechnical engineering. *Géotechnique*, 60(1), 3–74.
[4] Sellers, P., Mintz, Y., Sud, Y., Dalcher, A., 1986. A simple biosphere model (sib) for use within general circulation models. *Journal of the Atmospheric Sciences*, 505–531.

MODELLING HETEROGENEOUS GEOMATERIALS IN A THERMO-HYDRO-MECHANICAL FRAMEWORK

Alfonso Rodriguez-Dono[1,2*], Yunfeng Zhou[1], Sebastia Olivella[1,2]

[1] Department of Civil and Environmental Engineering, Universitat Politècnica de Catalunya, Barcelona, Spain

[2] International Centre for Numerical Methods in Engineering (CIMNE), Barcelona, Spain

* Corresponding author: Alfonso Rodriguez-Dono. E-mail: alfonso.rodriguez@upc.edu

Keywords: Heterogeneity; THM; CODE_BRIGHT; Coupled problems; Anisotropy; Porosity

Abstract. *A new approach to model coupled thermo-hydro-mechanical (THM) problems considering geomaterials with heterogeneous properties has been implemented in CODE_BRIGHT. It provides the possibility of considering geomaterials with a spatially correlated heterogeneous field of porosity, following a normal distribution. This spatial correlation can be isotropic or anisotropic. Material properties such as intrinsic permeability, thermal conductivity, diffusivity, retention curve, elastic modulus or cohesion are defined as a function of porosity and, hence, they become heterogeneous. A validation exercise has been carried out. The results, which have been compared with a homogeneous case, show that considering heterogeneous fields can be relevant in different modelling problems, especially coupled thermo-hydro-mechanical problems.*

1. INTRODUCTION

It is well known that geomaterials are heterogeneous. Under THM conditions, parameters such as thermal conductivity, intrinsic permeability, Young's modulus, etc. are affected by the distribution and properties of constituent minerals and bulk density. Hence, considering heterogeneity may be relevant when modelling the THM coupled behaviour of geomaterials, although it is usually ignored[i].

2. THEORETICAL BACKGROUND

The development of a spatially correlated heterogeneous field of porosity is based on the work of Davis[ii], following the geostatistical theory and using the LU triangular decomposition technique. The spherical semi-variogram has been chosen as the basis for the implementation in CODE_BRIGHT[iii] since perhaps it is the most commonly used semi-variogram model[iv]. In the spherical semi-variogram, C_0 is the nugget, which is due both to measurement errors and to micro-variabilities of the mineralization. a denotes the range, which means that any data value will be correlated with any other value falling within a radius a (as shown in Fig. 1). This spatial correlation is 'geometrically isotropic' if the range is constant, but can be said to be "geometrically anisotropic" when the range a varies with the direction, forming an ellipse (in 2D) or an ellipsoid (in 3D).
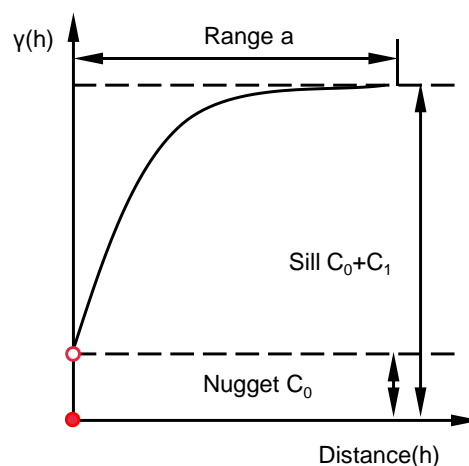
Figure 1. Semi-variogram model.

3. PROPOSED APPROACH FOR GENERATING HETEROGENEOUS FIELDS

Many parameters in CODE_BRIGHT can be a function of porosity, which means heterogeneous features are inherited automatically. In addition, it was found that the pore size distribution of some rocks (e.g. COx), approximately follow a normal distribution[v]. These reasons led to the selection of porosity as the variable used to generate a spatially correlated field following a normal distribution (Fig. 2). A specific module has been developed in CODE_BRIGHT to generate a spatially correlated heterogeneous field of porosity, following a Gaussian random distribution of mean μ and standard deviation σ (Fig. 2a).
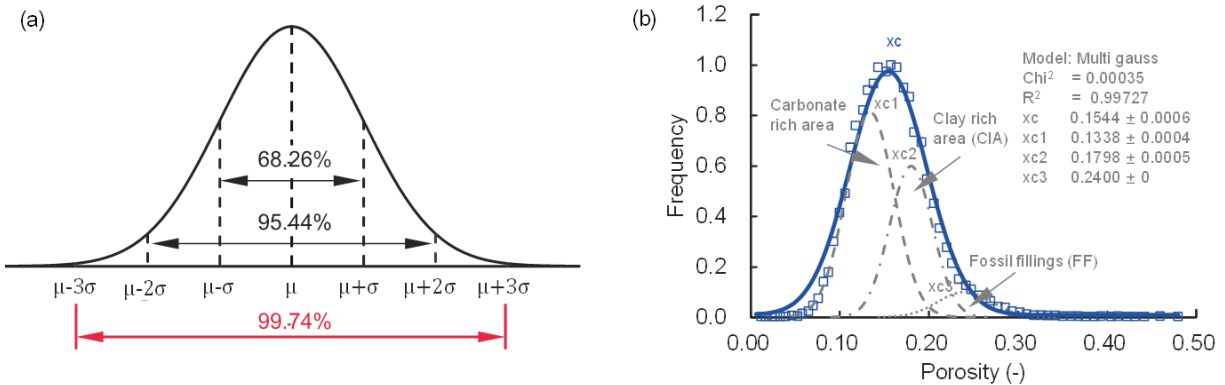
Figure 2. Normal porosity distribution: (a) Schematic diagram of the probability density curve; (b) Porosity histogram of a claystone, according to Sammartino et al. (2002) and modified from Géraud et al. (2007).

It is possible to determine semi-variograms from dry density measurements in samples[vi] or in-situ experiments[vii]. Thus, the basic parameters (variance, mean, range, etc.) of the semi-variogram can be estimated and, hence, the heterogeneous field is generated[i]. In modelling complex fluid injection problems, intrinsic permeability can be considered as the sum of two terms. The first one (k_{matrix}) is a function of the porosity of the matrix of the material according to Kozeny's law or to a calibrated exponential law (Fig. 3 left). Note that exponential law has been found to represent more accurately the intrinsic permeability of some geomaterials (e.g. bentonite). The second term ($k_{fracture}$) corresponds to the permeability associated with the aperture b of embedded fractures, according to a cubic law[viii]. These small micro-fractures or openings may develop in the material leading to preferential flow paths. Thus, this approach permits differentiating between the intrinsic permeability associated with the matrix and with the fractures[ix].
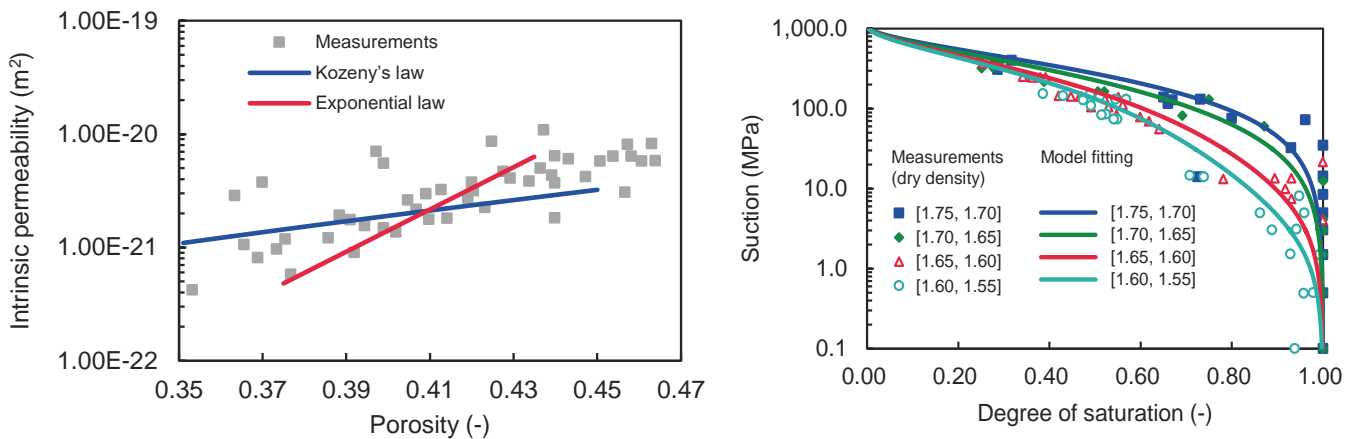
Figure 3. Left: Variation of intrinsic permeability with porosity[x]. Right: Retention curves for different initial dry densities[xi].

Furthermore, the retention curve is defined according to Van Genuchten's model, where the capillary pressure parameter can be considered a function of intrinsic permeability[i]. Hence, the retention curve varies with porosity. Fig. 3 (right) displays different retention curves for bentonite with different dry densities, which are functions of porosity. Note that different porosities give different retention curves according to the experimental data and, thus, a heterogeneous porosity distribution will result in a distribution of retention curves along the model.

Thermal conductivity is used in Fourier's law to compute conductive heat flux. Among other possibilities, empirical equations of the thermal conductivity as a function of porosity could be used[xii]. Fig. 4 (left) indicates that there is a dependency of the thermal conductivity on porosity. Therefore, a heterogeneous distribution of porosity will result in a heterogeneous distribution of thermal conductivity.
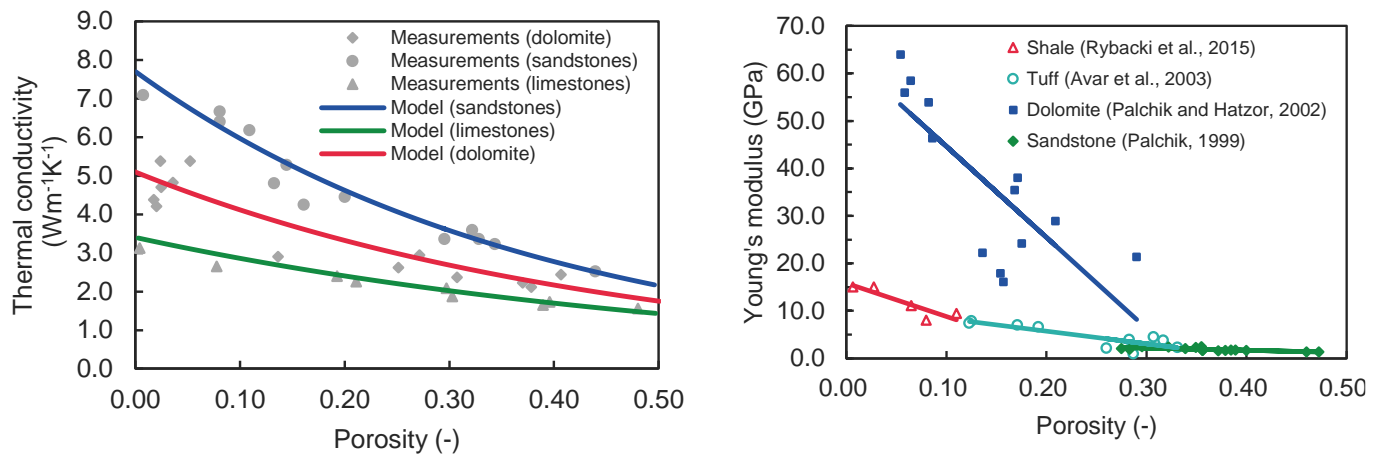
Figure 4. Left: Experimental data[xiii] and adopted model for thermal conductivity of different sedimentary rocks. Right: Young's modulus as a function of porosity for different geomaterials

Moreover, diffusion process is modelled using Fick's law[xiv], in which diffusive flux depends on porosity. Hence, a heterogeneous distribution of porosity will result in a heterogeneous distribution of diffusivity. Thus, the coefficient of effective diffusion can undergo variations in space and time.

Regarding mechanical properties, the experimental work of different authors shows a correlation between elastic moduli and porosity (Fig. 4 right), at least for some rocks. Therefore, in some cases it can be considered that the Young's modulus dependent on porosity follows a linear law. This approach may be useful to represent monotonic loading processes, as irreversibility is not well represented.

On the other hand, some models use internal variables linked to deformation (e.g. hardening/softening as a function of accumulated plastic strain). However, how to know the accumulated plastic strain in a sample before it is tested is an issue that remains unsolved. This could justify the introduction of porosity as a measure of the internal structure of the material, since porosity can be measured independently of the history of the material. In the context of crack formation by desiccation, the cohesion c has been considered a function of porosity[xv].

4. VALIDATION OF THE APPROACH

The validation of the proposed approach is presented in this section by comparison with laboratory measurements from gas injection tests on compacted bentonite, carried out by the British Geological Survey. Details of the testing apparatus can be found in Daniels and Harrington[xvi].

Using CODE_BRIGHT, a 3D coupled two-phase flow hydro-mechanical elastic model is considered, based in Damians et al.[ix]. In general, the geometry, boundary conditions and material parameters used are the same as in Damians et al.[ix], unless otherwise specified in this article. The main difference is that, in this case, a heterogeneous porosity field is generated with a mean porosity of 0.45 and a standard deviation of 0.033, which means a porosity range approximately between 0.35 and 0.55 (Fig. 5 left), with a range a = 0.04 m for spatial correlation, meanwhile in Damians et al.[ix] the porosity is considered constant and a heterogeneous permeability field is manually generated using different materials *ad hoc*.

In our model, the average initial intrinsic permeability k_0 is 3.3×10^{-21} m^2, matching the measurements of the experiment, and the change of the intrinsic permeability of the matrix with porosity has been modelled using the exponential law. Thus, due to the heterogeneous porosity field, initial intrinsic permeability of the matrix ranges between 1×10^{-22} m^2 and 1×10^{-19} m^2, approximately. Moreover, capillary pressure changes with porosity. In addition, an embedded fracture model properly calibrated has been used. Note that porosity does not change much during the experiment, due to material stiffness and constant volume test conditions. Therefore, the exponential law has an influence mainly in the initial intrinsic permeability, meanwhile the cubic law enhances the permeability in function of the strain locally developed.
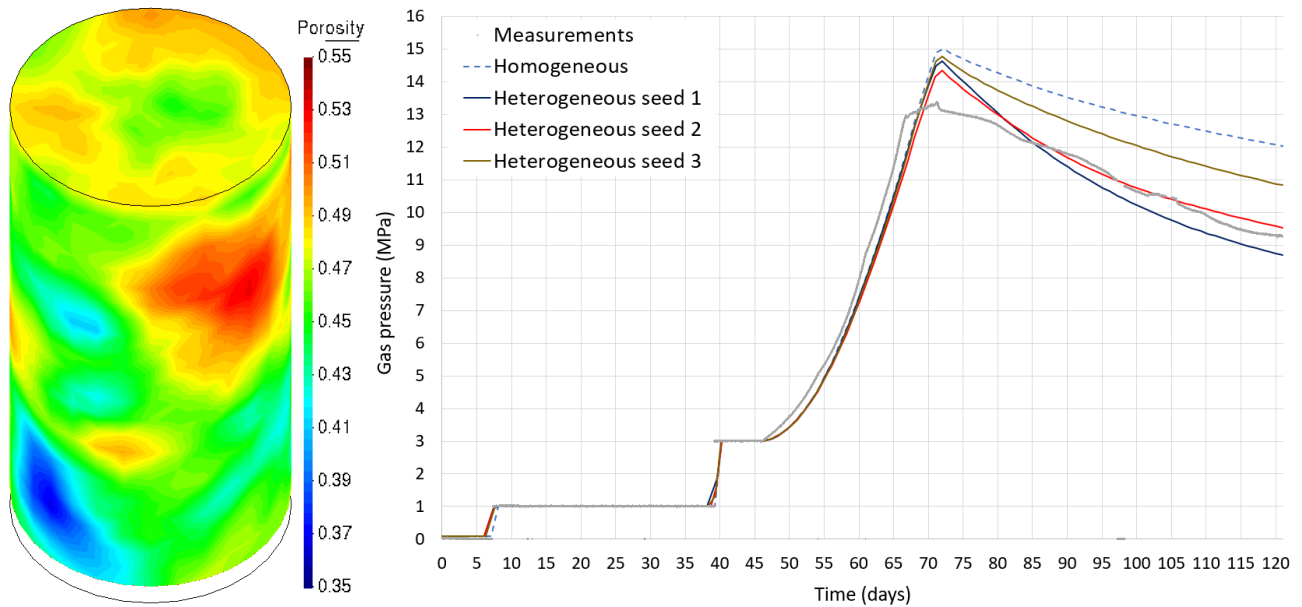
Figure 5. Left: geometry of the model and initial porosity distribution assumed for the bentonite in one of the models (heterogeneous seed 2). Right: Evolution of the gas injection pressure in the different cases.

Gas injection has different stages. Initially, the injection pressure is prescribed and after day 46 the flow rate is prescribed and, hence, gas pressure is calculated[ix]. Three heterogeneous identical models –with different seed– have been run and results are compared with measurements and with a homogeneous case in which initial porosity=0.45. The comparison (Fig. 5 right) shows a good correlation between model and experimental results, especially in the case of seed=2. Some variability depending on the seed is shown, particularly in terms of gas dissipation and less relevant concerning gas breakthrough pressure, which is slightly higher than in the experiment measurements. Nonetheless, a better matching compared to the homogeneous case is observed. An enhanced permeability gas path due to the aperture of discontinuities can be observed in the heterogeneous case s (Fig. 6), meanwhile in the homogeneous case the gas flows homogeneously through the sample.

Regarding the outflow, Fig. 7 (left) shows the comparison between the heterogeneous and the homogeneous models and the measurements. It is observed that the results are not far from the measurements, although the peak in the outflow rate is not completely recovered. This could be due to the use of an elastic model (as in Damians et al.[ix]). It is likely that considering inelastic deformations the results can get closer to the measurements, although this is beyond the scope of this validation exercise of the heterogeneous approach. Again, some variability can be observed among the three heterogeneous models, which seems to reproduce a slight peak that the homogeneous model is not able to reproduce.

Furthermore, plotting the gas volume being dissipated through the outflow side of the specimen, and comparing it with the measurements (Fig. 7 right), it can be observed that the total volume recovered according to the heterogeneous cases is in the range of the measured volume (specifically between seed 2 and 3 cases). This shows that the spatial distribution of the heterogeneity is relevant for the results obtained. On the other hand, the numerical models do not recover completely the gas volume increase rate observed around 70 days, which might be due to the fact that inelastic deformations are not considered.
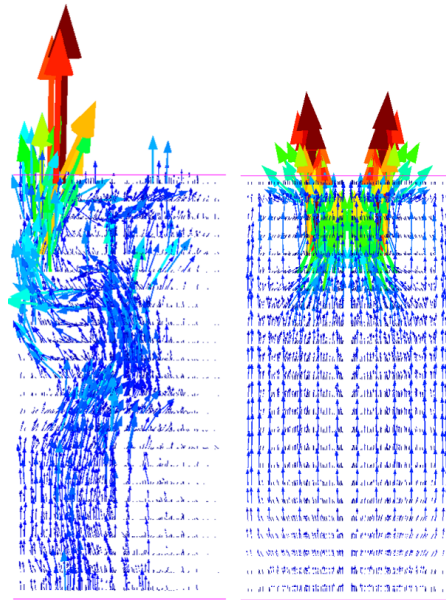
Figure 6. Gas path in heterogeneous (left) and homogeneous (right) cases.
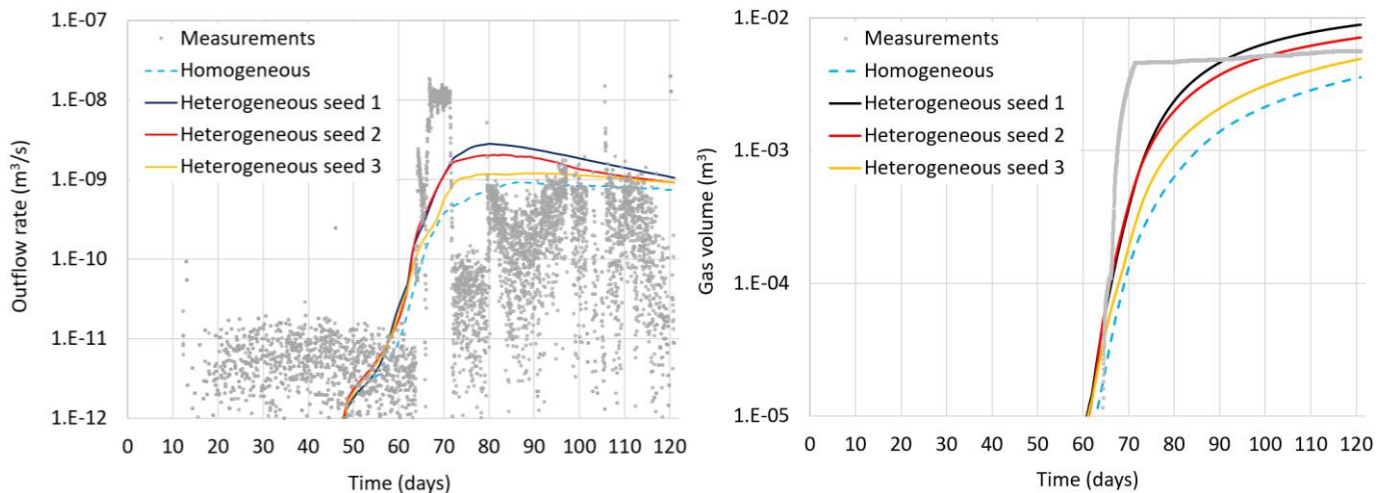
Figure 7. Left: Evolution of the outflow rate in different cases. Right: Evolution of the gas volume dissipated in different cases.

5

6. SUMMARY AND DISCUSSION

In this article, we present a new approach to perform THM calculations in a more realistic way by using information of the spatial distribution of density. The main idea in this approach is that an internal variable is used to develop a spatial variability, which acts as initial condition and in turn permits to calculate a spatial variability of other properties if dependence with porosity can be established. The internal variable is porosity, which can be calculated from dry density as it is better measured by image techniques.

The model has been validated showing a reasonable comparison with laboratory measurements. To illustrate some capabilities of the approach, we have shown that it can be relevant when modelling heterogeneous geomaterials. In particular, it has been demonstrated that the gas path in an in-situ gas injection test can be highly affected by a moderate heterogeneous distribution of porosity. These effects –we believe– could be relevant in different projects such as methane underground storage or CO_2 underground sequestration, fracking, geothermal, underground nuclear waste disposal, etc.

Therefore, the aim of the article is to provide a tool that may be useful in many THM cases to improve predictions or to provide a range of possible results by doing a handful of realizations with different distributions of porosity. The different distributions of porosity taken to perform the models can have the same or different mean or variance, and the same or different range for spatial correlation. Nonetheless, it is possible to use different distributions of porosity with the same mean, variance and range, just by changing the seed. The current approach may be especially relevant when dealing with clay-based geomaterials. A more detailed information, including additional examples, can be found in Rodriguez-Dono et al.[i].

References

[i]   Rodriguez-Dono A, Zhou Y, Olivella S, 2023. A new approach to model geomaterials with heterogeneous properties in thermo-hydro-mechanical coupled problems. Computers & Geotech., 159. https://doi.org/10.1016/j.compgeo.2023.105400
[ii] Davis, M. W., 1987. Production of conditional simulations via the LU triangular decomposition of the covariance matrix: Mathematical geology, v. 19, no. 2, p. 91-98.
[iii] Olivella, S., Gens, A., Carrera, J., and Alonso, E., 1996. Numerical formulation for a simulator (CODE_BRIGHT) for the coupled analysis of saline media: Engineering computations, v. 13, no. 7, p. 87-112.
[iv] Isaaks, E. H., Isaaks, D. A. E. S. E. H., Srivastava, R. M., and Knovel, 1989, Applied Geostatistics, Oxford University Press.
[v]   Armand G, Conil N, Talandier J, Seyedi DM, 2017. Fundamental aspects of the hydromechanical behavior of Callovo-Oxfordian claystone: from experimental studies to model calibration and validation. Computers & Geotechnics, 85:277-286.
[vi] Toprak, E., Olivella, S., and Pintado, X., 2020. Modelling engineered barriers for spent nuclear fuel repository using a double-structure model for pellets. Environmental Geotechnics, https://doi.org/10.1680/jenge.17.00086
[vii] Rodriguez-Dono A; Olivella S; Mokni N, 2020. Assessment of a high-level spent nuclear fuel disposal model. Environmental Geotechnics v. 7, no. 1, p. 42–58. https://doi.org/10.1680/jenge.18.00017
[viii] Olivella, S., and Alonso, E., 2008. Gas flow through clay barriers: Geotechnique, v. 58, no. 3, p. 157-176.
[ix] Damians, I., Olivella, S., and Gens, A., 2020. Modelling gas flow in clay materials incorporating material heterogeneity and embedded fractures: International Journal of Rock Mechanics and Mining Sciences, v. 136, p. 104524.
[x]   Sánchez, M., Gens, A., and Olivella, S., 2012, THM analysis of a large-scale heating test incorporating material fabric changes: International Journal for Numerical and Analytical Methods in Geomechanics, v. 36, no. 4, p. 391-421.
[xi] Gens A, Sánchez M, Guimarães LdN, Alonso E, Lloret A, Olivella S, Villar M, Huertas F, 2009, A full-scale in situ heating test for high-level nuclear waste disposal: observations, analysis and interpretation: Géotechnique, v. 59, no. 4, p. 377-399.
[xii] Olivella S, Vaunat J, Rodriguez-Dono A, 2022. CODE_BRIGHT User's Guide. Dep. Civil and Environmental Eng., UPC.
[xiii] Brigaud, F., and Vasseur, G., 1989, Mineralogy, porosity and fluid control on thermal conductivity of sedimentary rocks: Geophysical Journal International, v. 98, no. 3, p. 525-542.
[xiv] Olivella, S., 1995, Nonisothermal multiphase flow of brine and gas through saline media [Ph.D. thesis: UPC].
[xv] Trabelsi, H., Jamei, M., Zenzri, H., and Olivella, S., 2012. Crack patterns in clayey soils: Experiments and modeling: International Journal for Numerical and Analytical methods in geomechanics, v. 36, no. 11, p. 1410-1433.
[xvi] Daniels, K. A., Harrington, J. F., 2017. The Response of Compact Bentonite during a 1D Gas Flow Test. British Geological Survey Open Report. Ref: OR/17/067.

MODELLING MULTIPHASE FLOW, HEAT TRANSPORT AND BENTONITE SWELLING IN A RADIOACTIVE WASTE REPOSITORY IN CLAY ROCK

M. Carme Chaparro[*]

[*] CSD Engineers AG, Schachenallee 29A, 5000 Aarau, Switzerland
E-mail: c.chaparro@csd.ch

Key words: Thermo-Hydro-Mechanical Processes, Radioactive Waste Disposal, Numerical Model

Abstract. *A 2D THM model of an engineered barrier system in clay rock has been developed to investigate the time needed to saturate the bentonite and the temperature of the system once the bentonite will be full water saturated. The numerical model solves the mass balance of water and gas, the energy balance, and the stress equilibrium. Canister corrosion is modelled as inflow of gas and outflow of water in liquid phase. Results show that the engineered barrier system will be saturated within the first 100 years, due to a relevant advective liquid flux towards the bentonite. At that time, the temperature will be about 90℃ at the canister-bentonite interface, and 40℃ at the host rock, 25 m away from the canister. The heat from the canister provokes a diffusive flux and an advective gas flux towards the host rock, which is relevant the first 40 years. Once the bentonite is full water saturated the gas dissolves into the liquid phase.*

1 INTRODUCTION

Geological disposal in deep bedrock repositories is the preferred option for long-term management of high-level radioactive waste. An engineered barrier system considering clay as major barrier could include: the waste matrix, the canister, the bentonite and the concrete liner. Initially, the bentonite will be undersaturated and the canister will be at elevated temperature, which will create a heat flux towards the concrete liner. At the same time, the groundwater will go through the concrete liner due to the hydraulic gradient, which is triggered by the high suction of the bentonite. Due to the high reactivity of the concrete, it will be altered, and early leachates from degrading cement or concrete are hyperalkaline (pH>13) and chemically reactive with the bentonite. The hyperalkaline plume will saturate the bentonite that will exhibit swelling pressure evolution under the confining conditions in conjunction with changes in the fluid transfer properties. Once, the bentonite will be saturated, the plume will interact with the canister causing anaerobic corrosion. In the literature, several long-term reactive transport models consider a constant temperature and the system initially full water saturated[i,ii,iii,iv]. However, the geochemical reactions that will occur will be controlled by the temperature of the system, which will vary with time. Hence, a thermo-hydro-mechanical model has been developed with the objective of determining the time needed to saturate the bentonite and the temperature once the bentonite will be full water saturated.

2 NUMERICAL MODEL

A 2D numerical model has been developed using CODE_BRIGHT[v], simulating an engineered barrier system at 500 m depth. The model lasts for 100'000 years. The geometry of the model considers the bentonite, the concrete liner, and argillite as host rock. The metal canister is modelled as boundary condition (Figure 1).
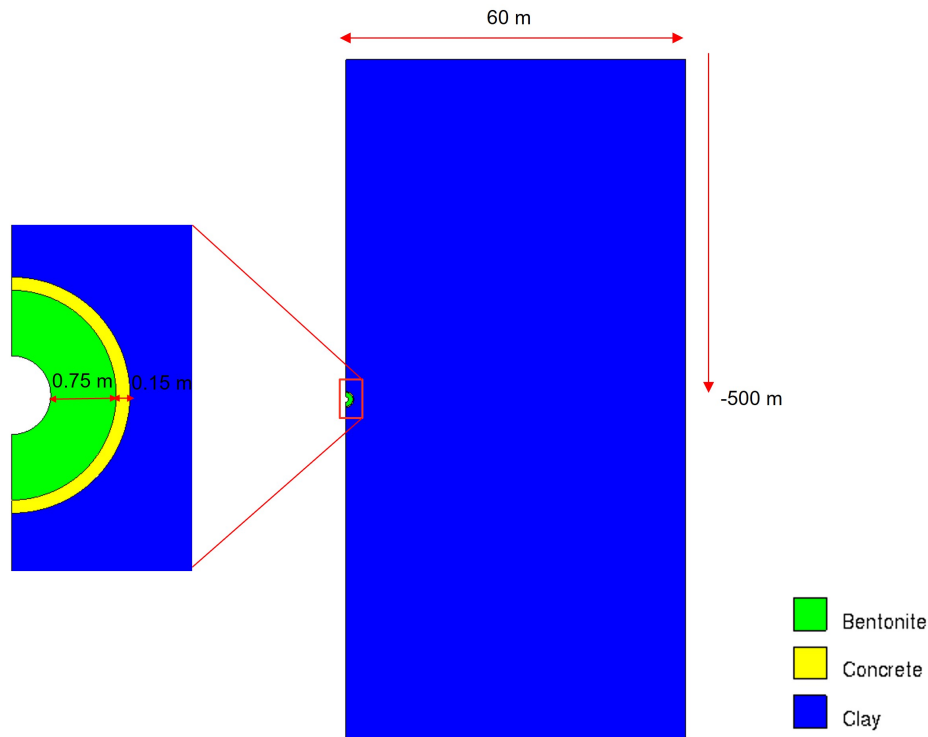
Figure 1: Geometry and materials of the 2D THM model

The conceptual model accounts for stress equilibrium, mass balance of water, mass balance of gas and energy balance. Allowing dissolved gas into liquid phase and vapour into gas phase. The thermo-elasto-plastic properties of the bentonite are the same as reported in literature[vi]. The linear elasticity and the main thermo-hydraulic properties of the materials are listed in table 1.

For initial conditions in the host rock, hydrostatic fluid pressure and a thermal gradient of 28ºC per km are assumed. The initial liquid pressure ranges from 4.3 to 5.5 MPa and the initial temperature from 22.3 to 25.7ºC. Initially, the bentonite and the concrete are undersaturated, with a saturation of 0.18 and 0.35 respectively. Isotropic stress is assumed being equal to the weight of the overburden rock, yielding a stress at the top boundary about -10.3 MPa. At the canister boundary, the temperature is prescribed and varies with time[vii]. Canister corrosion is modelled as inflow of gas (2.938e-11 kg/s) and outflow of liquid (2.644e-10 kg/s) at the boundary, representing the gas generation and the uptake of water respectively.

The mesh consists of 3140 nodes and 2998 quadrilateral elements, being more discretised at the interface canister-bentonite, bentonite-concrete and concrete-clay.

	Bentonite	Concrete	Clay rock
Density (kg/m^3)	2700	2700	2700
Porosity	0.46	0.07	0.137
Intrinsic permeability (m^2)	3.5e-20	1e-19	3.16e-20
Retention curve			
Entry pressure (MPa)	10	10	11
Shape function	0.4	0.33	0.29
Diffusive flux of vapour			
Vapour diffusion coefficient (m^2/s)	3.7e-6	7e-7	1.4e-6
Thermal properties			
Thermal conductivity (W/m/K)	0.35-1.3	2	1.2-1.9
Thermal expansion coefficient (^{o}C^{-1})	2.5e-5	1e-6	1.7e-5
Specific heat (J/kg/K)	893	900	800
Elastic constitutive law			
Young Modulus (MPa)	-	3e5	4e3
Poisson's ration	0.2	0.3	0.24

Table 1: Linear elasticity and thermo-hydraulic properties of the materials used in the THM model.

3 RESULTS AND DISCUSSION

Figure 1 shows the evolution of liquid pressure, gas pressure, temperature, and saturation. At the interface canister-bentonite, the liquid pressure decreases considerably due to evaporation provoked mainly by the heat at the canister. Gas pressure increases not only at the canister-bentonite interface, but also at the bentonite and concrete until the system gets full water saturated. Once the engineered barrier reaches the full water saturation, gas dissolves into water. The system reaches the full water saturation within the first 100 years, which is consistent with other similar models reported in literature[viii]. At that time, the temperature at the canister-bentonite interface is about 90ºC and about 40ºC at the clay rock, at 25 m away from the canister-bentonite interface.

During the water saturation period, there is a relevant advective flux of liquid from the clay rock towards the bentonite with a maximum of about 5e-7 kg/s, which is provoked for the hydraulic gradient. Near to the concrete-clay interface saturation in the clay rock decreases due to this strong gradient towards the bentonite.

Evaporation of water due to the heat yields a diffusive flux from the canister-bentonite interface to the host rock, which becomes especially relevant at 40 years, with a maximum of 3.5e-8 kg/s. In addition, there is an advective gas flux towards the clay rock mainly during the first 10 years, with a maximum of 6e-9 kg/s.
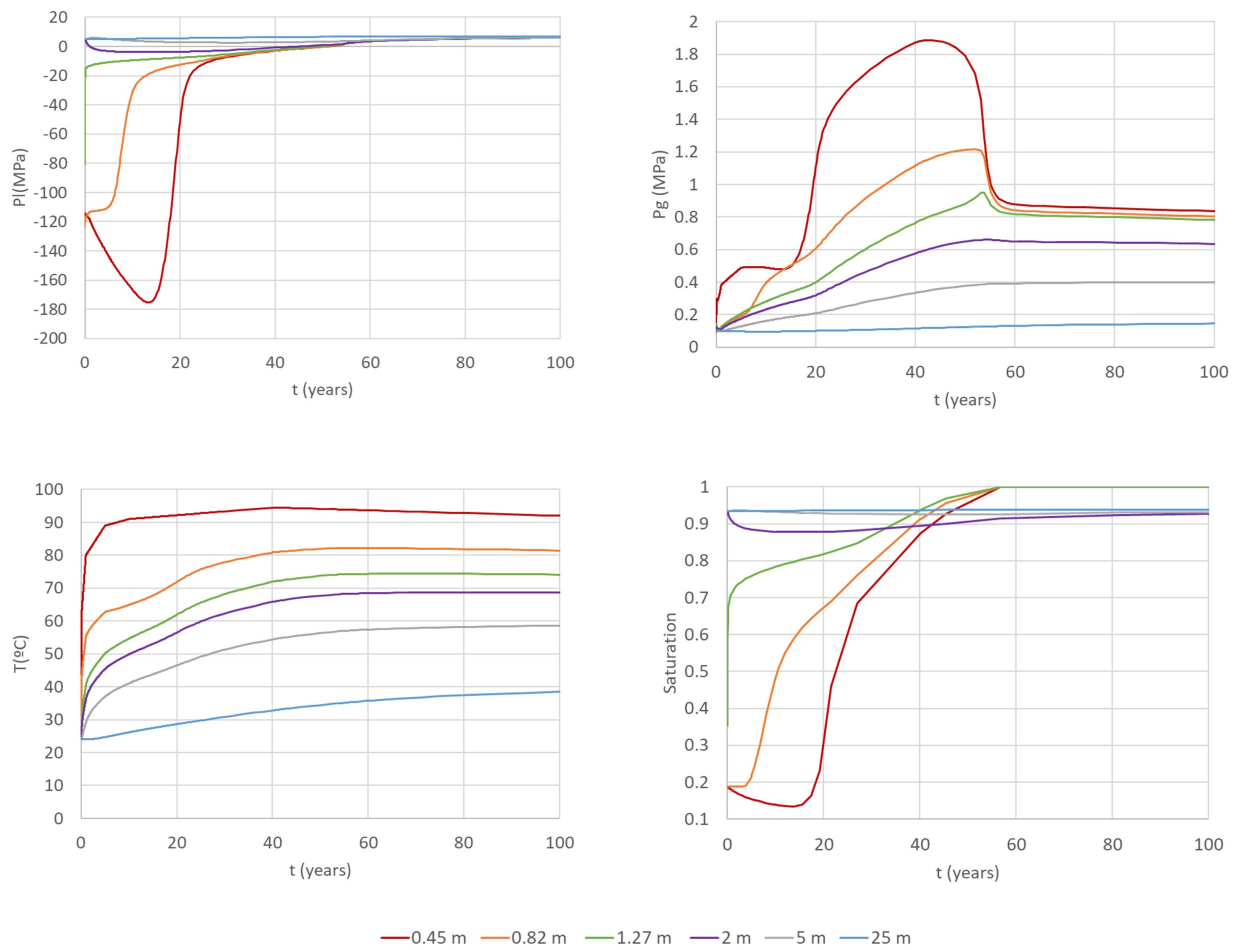
Figure 2: Evolution of liquid pressure, gas pressure, temperature and saturation calculated by the THM model. Coloured lines indicate results at different distances: canister-bentonite interface (0.45 m), bentonite (0.82 m), concrete (1.27 m) and host rock (2 m, 5 m, 25 m).

4 CONCLUSIONS

- Results of the 2D THM model reveal that the engineered barrier would be saturated within the first 100 years, due to a relevant advective liquid flux towards the bentonite.
- Once the bentonite is full water saturated, the temperature at the canister-bentonite interface is about 90ºC and 40ºC at the clay rock, 25 m away from the canister-bentonite interface.
- The heat at the canister-bentonite interface provokes a diffusive flux and advective gas flux towards the host rock, which is relevant during the first 40 years.
- When bentonite is water saturated, gas dissolves into the liquid phase.
- Results obtained in this study are sensitive to the THM properties of the materials and to the assumptions considered in the conceptual model.

REFERENCES

[i] Chaparro, M.C., N. Finck, V. Metz, H. Geckeis, 2021. Reactive Transport Modelling of the Long-Term Interaction between Carbon Steel and MX-80 Bentonite at 25ºC. Minerals, 11, 1272. doi:10.3390/min11111272.

[ii] Bildstein, O., L. Trotignon, M. Perronnet, M. Jullien, 2006. Modelling iron-clay interactions in deep geological disposal conditions. Physics and Chemistry of the Earth, Parts A/B/C, 31, 618-625. doi:10.1016/j.pce.2006.04.014.

[iii] Wilson, J.C., S. Benbow, H. Sasamoto, D. Savage, C. Watson, 2015.Thermodynamic and fully-coupled reactive transport models of a steel-bentonite interface. Applied Geochemistry, 61, 10-28. doi: 10.1016/j.apgeochem.2015.05.005.

[iv] Samper, J., A. Naves, L. Montenegro, A. Mon, 2016. Reactive transport modelling of the long-term interactions of corrosion products and compacted bentonite in a HLW repository in granite: Uncertainties and relevance for performance assessment. Applied Geochemistry, 67, 42-51. doi:10.1016/j.apgeochem.2016.02.001.

[v] Olivella, S., A. Gens, J. Carrera, E. E. Alonso, 1996, Numerical Formulation for a Simulator (CODE_BRIGHT) for the Coupled Analysis of Saline Media, Engineering Computations, 13 (7), 87-112.

[vi] Gaus, I., B. Garitte, R. Senger, A. Gens, R Vasconcelos, J.L. Garcia-Sineriz, T. Trick, K. Wieczorek, O. Czaikowski, K. Schuster, J.C. Mayor, M.Velasco, U. Kuhlmann, M.V. Villar, 2014. The HE-E Experiment:Lay-out, Interpretation and THM Modelling, Nagra Report NAB 14-53.

[vii] Rutqvist, J, 2020. Thermal management associated with geologic disposal of large spent nuclear fuel canister in tunnels with thermally engineered backfill. Tunnelling and Underground Space Technology, 102, 103454. doi: 10.1016/j.tust.2020.103454.

[viii] Wissmeier, L., G. Mayer, 2022. Multi-phase flow and heat transport modelling of a repository drift for high-level waste during operating and post-closure phases using PFLOTRAN, 8th International Conference on Clays in Natural and Engineered Barriers for Radioactive Waste Confinement, France.

IDENTIFICATION OF WATER RETENTION CURVE FROM FREEZING TEST

A. Macias. K. Bockova and J. Vaunat[*]

[*] Department of Civil and Environmental Engineering Technical University of Catalonia (UPC)
Campus Nord UPC, 08034 Barcelona, Spain
E-mail: jean.vaunat@upc.edu

Key words: Water retention curve, Freezing and thawing, capillary inhibition, numerical modelling.

Abstract. *In order to evaluate the thermo-hydraulic behaviour of geological materials subjected to freezing and thawing cycles, modelling work has been carried using a thermodynamic framework and constitutive relationships, A series of axisymmetric models were developed accounting for soil properties and laboratory test characteristics. Results give insights into key aspects of freezing/thawing phenomenon such as the relationship existing between time evolution of temperature and soil water retention curve.*

1 INTRODUCTION

Surficial erosion processes may develop in hard clays formations as the result of material degradation under climatic cycles. A typical yearly cycle consists in: 1) the degradation of the hard clay at the surface of the slope due to freezing and thawing (F-T) cycles during winter; 2) the granularization of the resulting mud under drying/wetting cycle during spring; 3) the transport of the granular upper crust during summer and autumn precipitations, which let intact material in contact to the atmosphere for the forthcoming cycle. In this paper, we focus on the very initial stage, i.e. the propagation of the freezing front in the soil, preliminary to any assessment of the thickness of degraded layer and the further evaluation of erosion volume.

2 GOVERNING EQUATIONS AND MODEL CHARACTERISTICS

F-T is a complex physical process resulting from several mechanisms. As temperature decreases, water starts to freeze in the soil pores and cryogenic suction develops, inducing water flow from the unfrozen to the frozen parts of the soil and resulting in material volume increase. Pore free water will freeze first because of the low level of grain-water interface energy to be overcome to create ice-water separation. Small pores will freeze at much lower temperatures because of the high capillary forces prevailing in it. Similarities can be established between these processes and the process of drying and wetting in unsaturated soils.

Following multiphase/multispecies approach[i]; in the scope of F-T processes, soil porous media is composed of two mass components: mineral grains (gr) and water (w), that can be described via four possible phases: solid (s), ice (i), gas (g) and liquid (l). Soil grains that correspond to solid phase constitutes the non-reactive skeleton of the medium, liquid phase can move and be storage in the available spaces that results from the solid phase composition, and ice can develop on the same spaces as phase change occurs over the liquid phase. For this model the following volumetric restrictions are in place on the multi-phase approach.

$$S_l + S_g = 1 \tag{1}$$

$$\frac{\phi_a}{\phi_p} = 1 - S_i \tag{2}$$

where S_l, S_g and S_i are the degrees of saturation in liquid, gas and ice, respectively. ϕ_p is the volume of pores / total volume and ϕ_p is the volume of pores no filled by ice over the total volume. Main processes taking place in the porous medium Are: mechanical deformation, fluid flow, thermal flow and phase change. Mechanical aspects will not be considered in this work.

2.1. Governing equations

The mathematical expressions that describe the different non-mechanical processes involved in the F-T processes are based on balance equations and constitutive relationships, constrained by the restriction sin volume previously defined. Balance equations include:

Mass balance of minerals:

$$\frac{\partial}{\partial t}\left(\rho_s\left(1 - \phi_p\right)\right) + \nabla\left(\boldsymbol{j}_s^{gr}\right) = 0 \text{ and } \boldsymbol{j}_s^{gr} = \rho_s\left(1 - \phi_p\right)\frac{\partial u}{dt} \tag{3}$$

Mass balance of water:

$$\frac{\partial}{\partial t}\left(\theta_l^w S_l \phi_a + \theta_i^w S_i \phi_p\right) + \nabla\left(\boldsymbol{j}_l^w + \boldsymbol{j}_i^w\right) = f^w \tag{4}$$

Energy balance equation:

$$\frac{\partial}{\partial t}\left(\left(E_l\rho_l S_l + E_g\rho_g S_g\right)\phi_a + E_i\rho_i S_i\phi_p + E_s\rho_s\left(1 - \phi_p\right)\right) \tag{5}$$
$$+ \nabla\left(\mathbf{i}_c + \mathbf{j}_{E_s} + \mathbf{j}_{E_i} + \mathbf{j}_{E_g} + \mathbf{j}_{E_l}\right) = f^Q$$

$$\boldsymbol{j}_{E_l} = \boldsymbol{i}_{E_l} + \boldsymbol{j}_l^w E_l^w + E_l\rho_l\phi_a S_l\frac{\partial \boldsymbol{u}}{\partial t} \tag{6}$$

$$\boldsymbol{j}_{E_g} = \boldsymbol{i}_{E_g} + \boldsymbol{j}_g^a E_g^a + E_g\rho_g\phi_a S_g\frac{\partial \boldsymbol{u}}{\partial t} \tag{7}$$

$$\boldsymbol{j}_{E_i} = E_i\rho_i\phi_p S_i\frac{\partial \boldsymbol{u}}{\partial t} \tag{8}$$

$$\boldsymbol{j}_{E_s} = E_s\rho_s(1 - \phi_p)\frac{\partial \boldsymbol{u}}{\partial t} \tag{9}$$

2.3. Constitutive equations and equilibrium constraints

The freezing characteristic function is obtained by substituting the Clausius-Clapeyron equation in the retention curve. Clausius-Clapeyron equation expresses the chemical equilibrium between species present in the different phases. The retention curve is defined in this work by the Van Genuchten's model[ii]. The resulting freezing

characteristic curve defines the relationship between ice saturation, liquid pressure and temperature according to:

$$S_i = 1 - \left\{ 1 + \left[\frac{1 - \left(1 - \frac{\rho_i}{\rho_l}\right) P_l - \rho_i L ln\left(\frac{T}{273.15}\right)}{P_{c0}} \right]^{\frac{1}{1-m}} \right\}^{-m} \tag{10}$$

3. WRC relationship and model results

As described previously, during a freezing test, the degree of saturation of ice will be controlled by the temperature propagation into the sample and the water pressure, according to the shape of the retention curve. As such, it is expected that temperature time evolution inside the sample can be directly related to the parameters of the retention curve. In Figure 1, a map is presented, which provides iso-error lines obtained by comparing the time evolution of temperature measured in an experimental freezing test and numerical simulations of the same test using different parameters of the retention curve (using van Genuchten expression). Test consists in placing a soil sample into a bath with controlled temperature. Water content is maintained constant during the test.
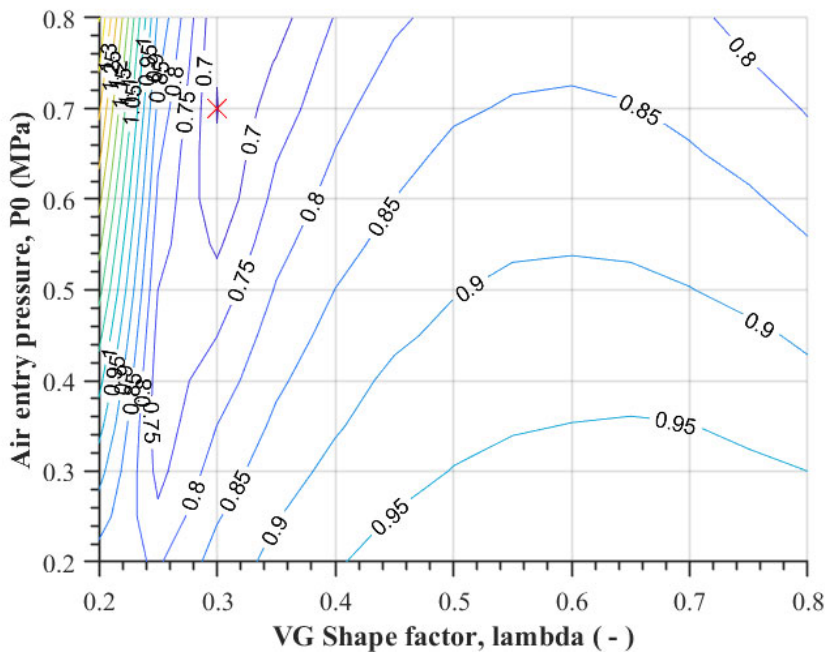
Figure 1. Contour lines for the temperature differences between the different SWRC models and laboratory results. Optimum air entry pressure and shape factor identified.

According to the calibration, best estimation of SWRC parameters (air entry pressure and shape factor) corresponds to values equal to 0.3 for the m parameter and p0 for the air entry pressure. Figure 2 shows a comparison between the best estimated SWRC and the retention curve identified in the laboratory for the tested soil.

The calibrated model allows getting insights into the development of ice saturation in the sample. As depicted in Figure 3, in a first stage, temperature at the center of the

sample monotonically decreases from initial (laboratory) temperature to 0. Afterwards, a plateau at 0ºC in temperature is observed, due to the heat consumed for water phase changes. Time evolution of degree of saturation indicates that 30% of pore water has frozen at the end of the plateau. It corresponds to the free water present in the large pores of the sample. To freeze the remaining water, located in small pores, higher negative temperatures are required. At -18ºC, 76% of pore water is frozen.
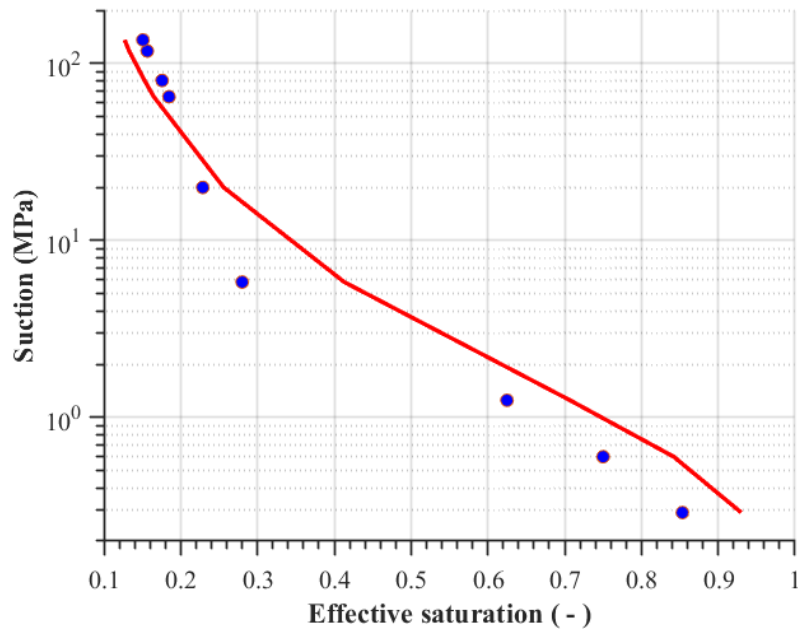
Figure 2 Comparison between the best-estimate of SWRC and the SWRC determined in the laboratory.
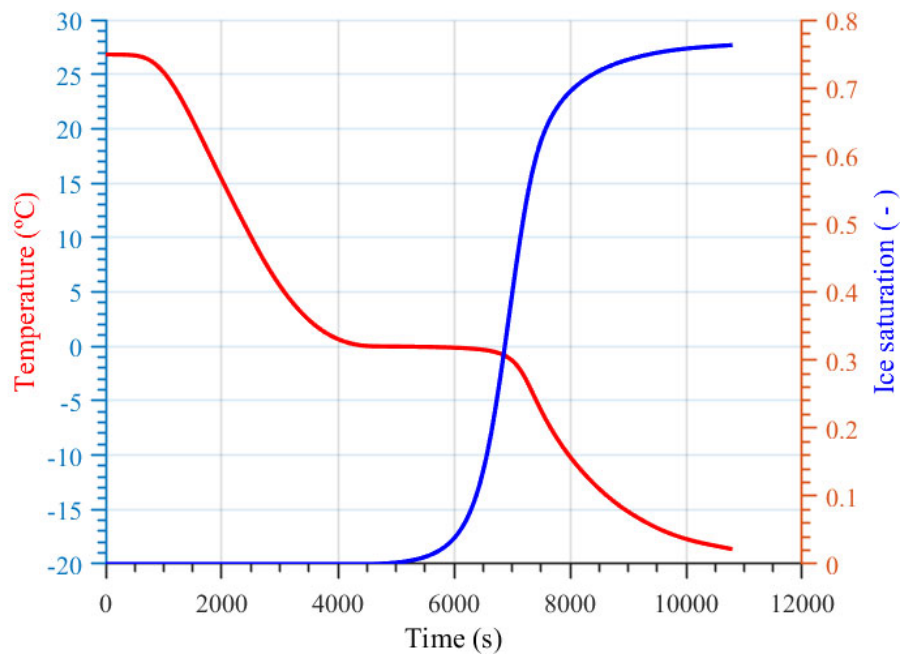
Figure 3. Time evolution of temperature and ice saturation at the center of the sample as obtained by the best estimated numerical model.
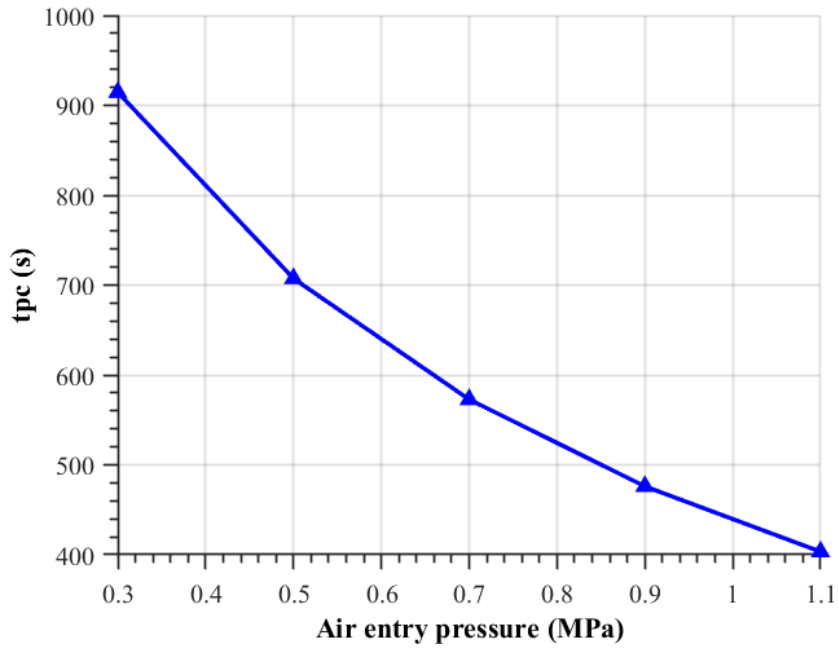
Figure 4. Relationship between duration of temperature plateau (tpc) and SWRC air entry pressure.
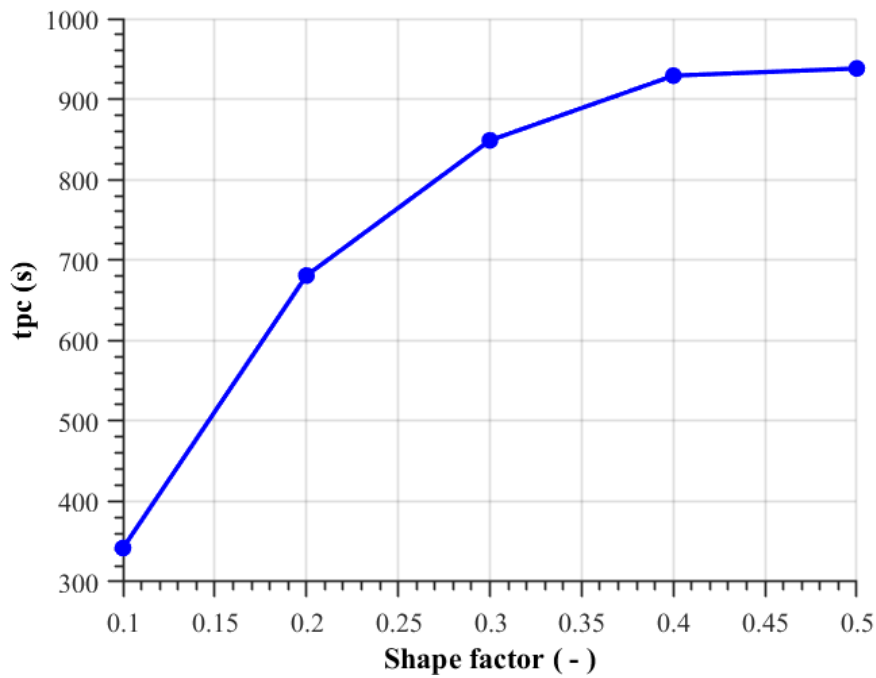
Figure 5. Relationship between duration of temperature plateau (tpc) and SWRC m parameter.

Figure 4 and 5 presents the correlation existing between the duration of temperature plateau (tpc) and van Genuchten SWRC parameters. A clear tendency is observed, which can be explained by the fact that the amount of free water (corresponding to the one that freezes at 0 ºC) is a highly representative point of the SWRC. Higher values

of tpc indicates that there is more free water in the sample and thus that p0 is lower and m is higher.

4. CONCLUSIONS

Numerical modeling to constitutes a useful tool to analyze the dynamics of freezing/thawing process in porous media, allowing for the determination of the relationship between SWRC and ice saturation. Morever, it allows for looking for relationship between temperature evolution, closely linked to water phase change, and the shape of the retention SWRC.

REFERENCES

i.   Olivella, S., Gens, A., Carrera, J., and Alonso, E. E. (1996). Numerical formulation for a simulator (code-bright) for the coupled analysis of saline media. Engineering Computations, 13(7):87–112.

ii.   Nishimura, S., Gens, A., Olivella, S., & Jardine, R. (2009). An elastoplastic model for the THM analysis of freezing soils. In *X International Conference on Computational Plasticity* (pp. 1-4).

COUPLED HYDROMECHANICAL MODELING OF THE INDUCED SEISMICITY AT THE ENHANCED GEOTHERMAL SYSTEM OF BASEL (SWITZERLAND)

Auregan Boyet[1,2,3], Silvia De Simone[3], Shemin Ge[4], Víctor Vilarrasa[1]

[1] Global Change Research Group (GCRG), IMEDEA, CSIC-UIB, Esporles, Spain
[2] Associated Unit: Hydrogeology Group (UPC-CSIC)
[3] Institute of Environmental Assessment and Water Research (IDAEA), CSIC, Barcelona, Spain
[4] University of Colorado Boulder: Boulder, Colorado, United States

Key words: Fractured rock, fault reactivation, slip weakening, dilatancy, numerical simulations

Abstract. *Induced seismicity hinders the acceptance and development of Enhanced Geothermal Systems (EGS). We study the case of the Basel EGS project using a hydromechanical model to simulate pressure and stress variations due to fluid injection. We are able to identify the combination of triggering mechanisms that induced seismicity at the study case. Effects of poroelastic stressing and static stress transfer are crucialin the explanation of the post-injection induced seismicity.*

1 INTRODUCTION

Enhanced Geothermal Systems (EGS) are developed to produce electricity from the production of hot water in the subsurface. A fluid is injected in a deep crystalline basement under a high pressure in order to enhance the permeability of the pre-existing faults and fractures. Hydraulic stimulations and hot water production induce seismicity that hinders the viability of EGS projects (Majer et al., 2007). The recent case of the post-injection induced seismicity at the EGS project in Pohang (South Korea, 2017) raised doubts about the viability of EGS projects (Ellsworth et al., 2019). The case of the Deep Heat Mining Project at Basel (Switzerland, 2006) has been well documented and is still controversial (Häring et al., 2008). After only six days of fluid injection, relatively large magnitude seismicity with a magnitude higher than the threshold set by local authorities felt by the population occurred, led to the stop of injection. Yet, the largest magnitude earthquake occurred five hours after the shut-in. We intend to explain the mechanisms inducing the seismicity during, but especially after the stop of injection.

2 METHODS

We study the triggering mechanisms of the seismicity solving the hydromechanical problem over a simplified two-dimensional faulting network designed from the monitored seismicity (Figure 1). Because the focal mechanisms of the monitored seismicity have a

vertical dip and a strike-slip movement, we assume a 2D plane-strain horizontal domain set at the depth of the injection well to reproduce the reactivation of the faulting network. We use the clustering work of Deichmann et al. (2014) to design the faulting network, as a function of their focal mechanisms, location and time of occurrence. Initial conditions and rock parameters are set as a function of the monitored and estimated data (Häring et al, 2008). We calibrate the friction coefficient to tune the fault reactivation with the monitored cumulative seismic moment of each cluster (Boyet et al., 2023). We estimate pore pressure and stress variations due to water injection solving the fully coupled hydromechanical problem with the Finite Element Method (FEM) simulator CODE_BRIGHT (Olivella et al., 1996), both during and after the stop of fluid injection. Fault elements are subject to a Mohr-Coulomb criterion with dilatancy and strain softening.
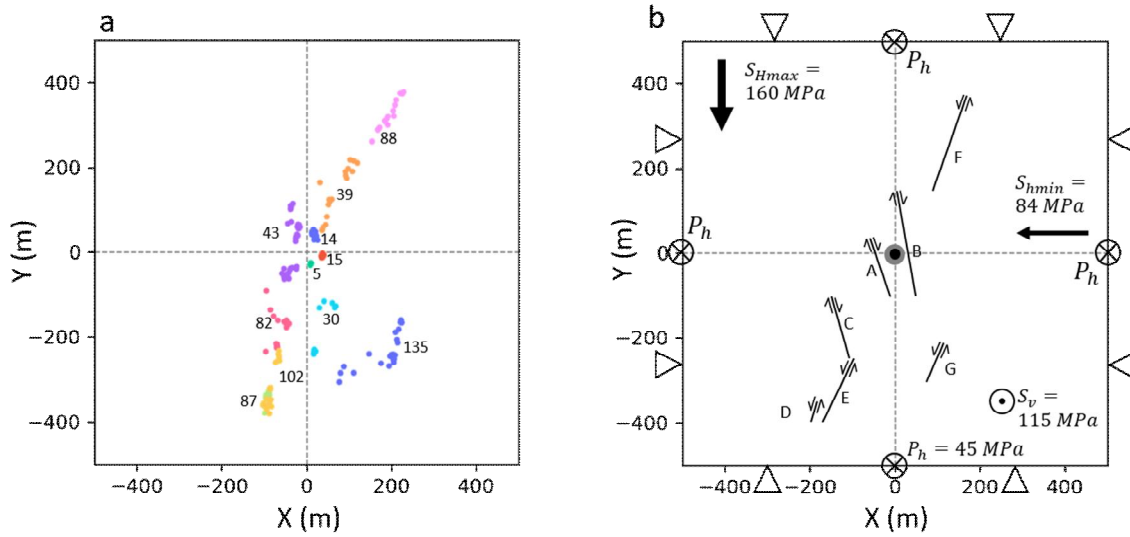
Figure 1 Design of the model. a) Location of monitored events, sorted by clusters projected at the depth of the well (Deichmann et al, 2014). b) Model of the faulting network based on the clusters of the monitored seismicity. Initial conditions and parameters are assigned based on known values and a calibration process

3   RESULTS

The modeled plastic strain of the different faults evolves according to the same trend as the monitored cumulative seismic moment at Basel. The strain-softening applied on the faults allows to simulate slip weakening and its effects on multiple fault reactivations (Figure 2d). Therefore, the model allows to identify the triggering mechanisms of fault reactivations. During injection, pore pressure diffusion is the dominant triggering mechanism of the faults in the vicinity of the well, while poroelastic stressing and stress redistribution affect farther areas (Figure 2a and b). After the stop of injection, pore pressure continues to diffuse in the domain but with a small magnitude. This pressure buildup can affect stability of faults that are not pressurized during injection after a long time. However, we observe that the abrupt stop of

injection induces a quick relaxation of the poroelastic stressing. Faults that are stabilized by poroelastic stressing during injection become destabilized after the stop of injection. Combined with static stress transfer from adjacent faults, faults can reactivate shortly after the stop of injection (Figure 2f). This process corresponds to the largest magnitude earthquake monitored in Basel.

4   CONCLUSION

This simplified hydromechanical model allows to better understand the complex combinations of mechanisms inducing the seismicity at the Basel EGS project. Co-injection induced seismicity is triggered by pore pressure buildup in the vicinity of the well. Farther, poroelastic stressing and static stress transfer trigger fault reactivation during and after the stop of injection.
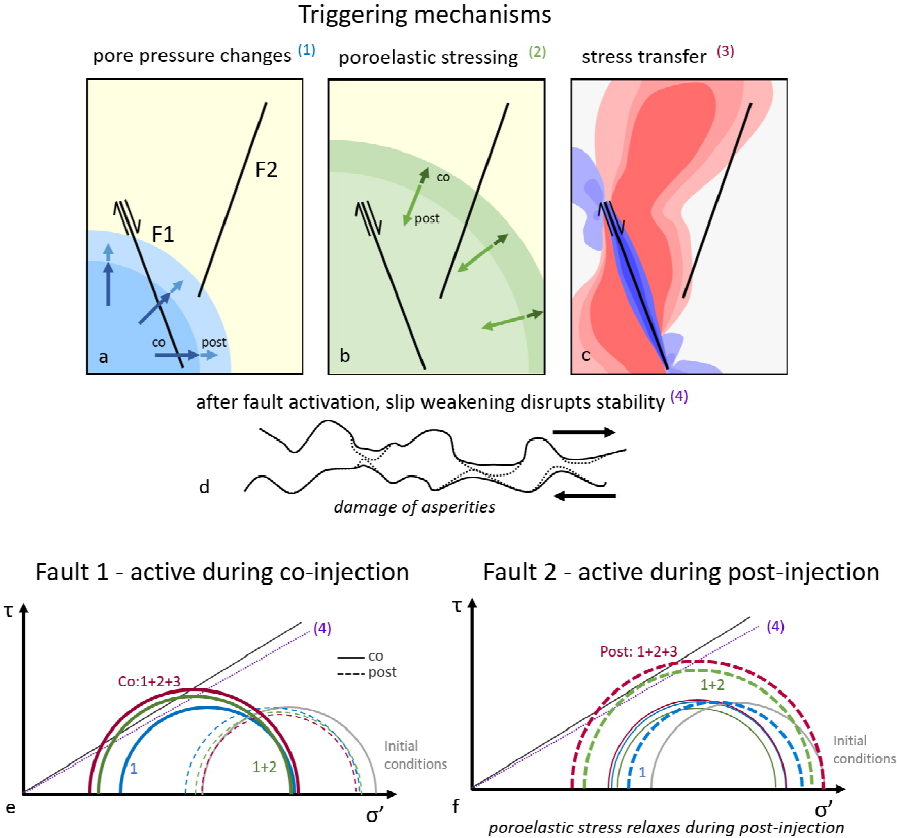
Figure 2 Conceptual illustration of triggering mechanisms: (a) Pore pressure buildup diffuses both during injection and post-injection stages, while (b) poroelastic stressing propagates farther and then contracts after the stop of injection. (c) Stress transfer due to shear slip of fault F1 disrupts the stability of the adjacent fault F2. (d) Fault asperities damage due to friction from fault activation weakens friction properties of the fault. (e) and (f) Mohr-Coulomb diagrams illustrating the combination of the three mechanisms on faults in the region of F1 and F2, respectively. Each colored circle represents the addition of a mechanism starting from the initial conditions. Solid circles represent co-injection mechanisms while dashed circles illustrate post-injection processes. In the region of F1 (e), pore pressure increase displaces the circle (solid blue) to the left during the injection, but failure on certain orientations is only driven if the effects of poroelastic stressing (solid green), slip stress transfer and

3

slip weakening (solid red) are considered. Shear-induced stress drop combined with pressure drops leads to more stable conditions in the post-injection. In the region of F2, (f), pore pressure changes are smaller and poroelastic stressing increases stability during injection, while after the stop of injection, poroelastic stress reduction, combined with stress transfer and slip weakening effects, leads to failure of faults with specific orientations.

REFERENCES

Boyet, A., De Simone, S., Ge, S., & Vilarrasa, V. (2023). Poroelastic stress relaxation, slip stress transfer and friction weakening controlled post-injection seismicity at the Basel Enhanced Geothermal System. *Communications Earth & Environment*, *4*(1), 104. https://doi.org/10.1038/s43247-023-00764-y

Deichmann, N., Kraft, T., & Evans, K. F. (2014). Identification of faults activated during the stimulation of the Basel geothermal project from cluster analysis and focal mechanisms of the larger magnitude events. *Geothermics*, *52*, 84–97. https://doi.org/10.1016/j.geothermics.2014.04.001

Ellsworth, W. L., Giardini, D., Townend, J., Ge, S., & Shimamoto, T. (2019). Triggering of the Pohang, Korea, Earthquake (Mw 5.5) by Enhanced Geothermal System Stimulation. *Seismological Research Letters*. https://doi.org/10.1785/0220190102

Häring, M. O., Schanz, U., Ladner, F., & Dyer, B. C. (2008). Characterisation of the Basel 1 enhanced geothermal system. *Geothermics*, *37*(5), 469–495. https://doi.org/10.1016/j.geothermics.2008.06.002

Majer, E. L., Baria, R., Stark, M., Oates, S., Bommer, J., Smith, B., & Asanuma, H. (2007). Induced seismicity associated with Enhanced Geothermal Systems. *Geothermics*, *36*(3), 185–222. https://doi.org/10.1016/j.geothermics.2007.03.003

Olivella, S., Gens, A., Carrera, J., & Alonso, E. E. (1996). Numerical formulation for a simulator (CODE_BRIGHT) for the coupled analysis of saline media. *Engineering Computations*, *13*(7), 87-112. https://doi.org/10.1108/02644409610151575

EXPLORING MATERIAL HETEROGENEITY IN GAS FLOW SIMULATION THROUGH CLAY MATERIALS: A NUMERICAL STUDY

Noghretab, B.S. [*†], Damians, I.P. [*†], Olivella, S. [*†], and Gens, A. [*†]

[*] Department of Civil and Environmental Engineering, Universitat Politècnica de Catalunya·BarcelonaTech (DECA-UPC)
Campus Nord UPC, 08034 Barcelona, Spain
E-mail: babak.sayad.noghretab@upc.edu

[†] International Centre for Numerical Methods in Engineering (CIMNE),
c/ Gran Capità S/N, 08034 Barcelona, Spain.

Key words: Hydro-gas coupled analysis, heterogeneity, permeability, CODE_BRIGHT

Abstract. *This paper presents the results of the initial molding of the large-scale gas injection test 1 (Lasgit) conducted at the Äspö Hard Rock Laboratory in Sweden. Lasgit is a field test that follows the Swedish KBS-3V disposal concept, in which copper/steel canisters containing spent nuclear fuel are deposited in disposal boreholes drilled into the repository tunnels' floor. Bentonite blocks are used to fill the space around each canister, which will eventually swell and seal any gaps. Once hydrated, the bentonite acts as a diffusional barrier to prevent the migration of radionuclides. The gas flow process is influenced significantly by material heterogeneity and local deformability, and material properties are not constant throughout. The initial medium structure is non-uniform, and deformations can result in changes in hydraulic properties and structure. Therefore, material heterogeneity is critical in the THM modeling process. To simulate the tests, a coupled hydro-gas-mechanical 3D numerical model was developed. The model assumes initial permeability to be heterogeneous and includes embedded fractures in the formulation. The model accurately reproduces the observed gas pressure evolution during the test.*

1 INTRODUCTION

Many countries that use nuclear energy have chosen to store their nuclear waste in geological formations for long-term confinement. One option is to bury the waste in a clay formation, but this can result in the generation of hydrogen and other gases due to the radioactive decay of the waste, radiolysis of water, and corrosion of metallic materials under anoxic conditions. If gas production exceeds the rate of gas diffusion within the clay pores, a discrete gas phase can form and accumulate until the gas pressure becomes large enough to exceed the surrounding material's entrance pressure. This can lead to a dilating and advective gas flow[i]. To properly design and layout any future facility, it is important to have a comprehensive understanding of the processes and mechanisms involved in gas flow and its impact.

Significant quantities of gases may be produced in underground radioactive waste repositories as a result of numerous processes, primarily the interaction of ground waters and brines with waste and designed materials in the disposal system. The gases may migrate

through the designed barrier system as well as the natural geological barrier in some circumstances. In the construction of safety cases for underground radioactive waste repositories, the potential impact of gas generation, accumulation, and migration on the performance of the various barriers, and, ultimately, on the long-term safety of a repository, should be addressed and analyzed[ii].

THM modeling of actual case studies regarding nuclear waste disposal or in situ testing scenarios, including gas migration in clays, is a topic that receives special attention today[i,iii].. The concepts of embedded fracture and heterogeneity were of key importance in reproducing preferential trajectories/paths induced by gas migration that develop under deformable flow conditions[iv,v].

The DECOVALEX project, which began in 1992, is an international research and model comparison partnership aimed at better understanding and modeling of coupled thermo-hydro-mechanical-chemical (THMC) processes in geological systems. LASGIT project, which stands for Large Scale Gas Injection Test, is a laboratory experiment of significant size that examines the behavior of gas flow in a clay formation. The experiment involves introducing gas into a block of bentonite, which allows observation of gas movement within the clay and measurement of pressure changes within the system[vi].

The numerical code for finite element calculations CODE_BRIGHT is the main research tool in this research. CODE_BRIGHT has been developed in the Department of Civil and Environmental Engineering (DECA) of the Universitat Politècnica de Catalunya·BarcelonaTech (UPC) and works in combination with the pre/post-processor GiD developed by the International Center for Numerical Methods in Engineering (CIMNE) where several pre-process tools are available (e.g., geometry generation and meshing) as well as 2D and 3D representation developments[vii].

2   METHODOLOGY AND MAIN MODEL FEATURES

2.1 Test Geometry

To assess the LASTGIT gas flow test 1, despite that the full-setup model was initially created with tetrahedral elements, just a quarter of the constructed model is represented and used for current draft computations (see Fig. 1).

2.2 Heterogeneity

In this study in the context of the modelling carried out, a coupled hydro-gas three-dimensional (3D) finite element method (FEM) model was created and implemented to assess the gas flow experiments. Initial permeability is assumed heterogeneous throughout the bentonite, pellet and gap layers, and embedded fractures are incorporated in the formulation.

A layer-by-layer random permeability distribution assumed in 3 different zones[v]: with $2/3-1/6-1/6$ weighting for intrinsic permeabilities equal to 1×10^{-21} m^2, 1×10^{-20} m^2 and 1×10^{-19} m^2 for bentonite, pellets, and gap considered with different embedded fracture parameters (Fig. 2). Although the full-setup model was initially created with tetrahedral elements, just a quarter of the constructed model is represented and used for computations. Since this model considered fully saturated, the initial porosity of bentonite, pellets and gap layers are constant (0.366, 0.706, and 0.366, respectively).
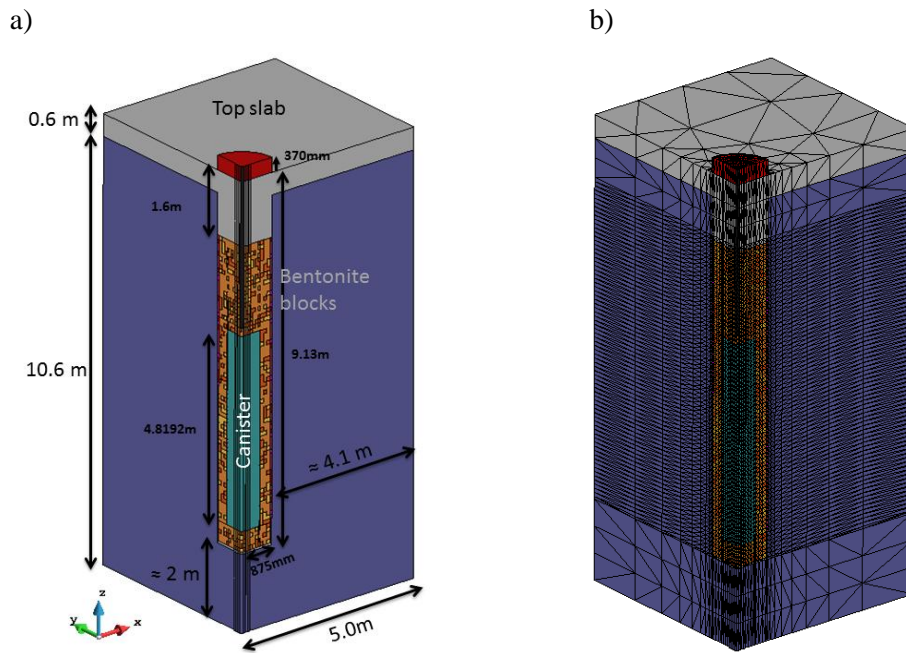
Figure 1. Model geometry: (a) general view and dimensions and (b) mesh (by 66948 tetrahedra and triangle elements with 13170 total nodes).
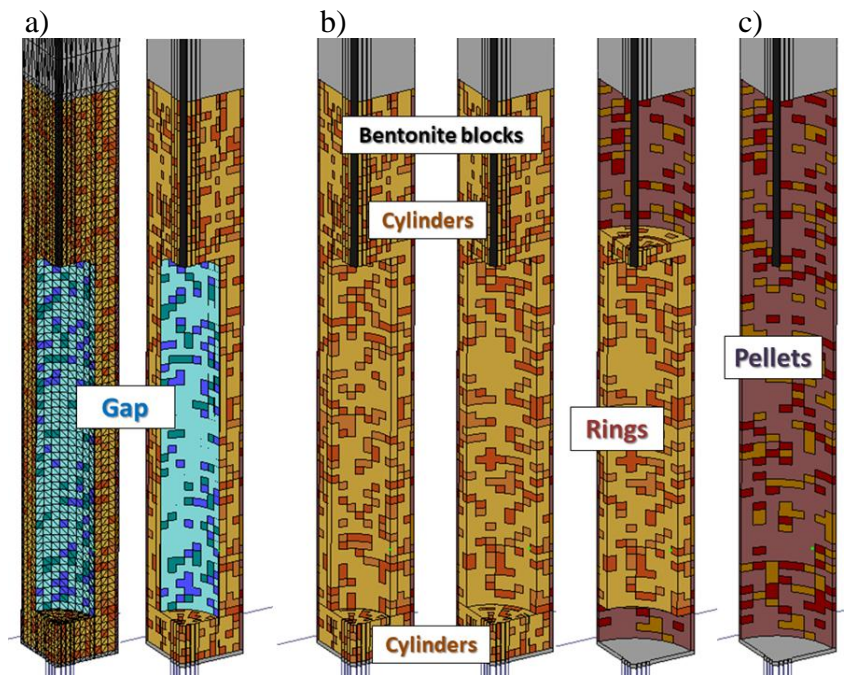
Figure 2. Hand-made heterogeneity propagation in (a) gap, (b) bentonite blocks (rings and cylinders), (c) pellets.

2.3 Model Features

The LASGIT Test 1 is modelled from day 0 to 1000, and the time frame for the test is divided into distinct intervals corresponding to different stages of the test. To ensure accurate results, an automatic time step control is used to limit the number of Newton-Rapson iterations within each interval. The maximum and minimum time steps are set to match the required time frame steps, ensuring that the results have sufficient time resolution.

Boundary conditions are modeled in agreement with the specified LASGIT set-up and injection filters are modeled based on the test descriptions for injection point FL903 for Gas Test 1. A volume factor was internally incorporated to take into account the effective volume of the injection system (i.e., vessel, pipework, etc.) enabling us to do a sensitivity on gas volume factor injection into the system to model the injection of the gas into the clay.

2.4 constitutive model and Equations

For the purposes of this study, a constitutive model that incorporates embedded permeability[iv] was utilized. The model decomposes intrinsic permeability into matrix and fracture terms, both of which vary with changes in porosity and aperture. In addition, the study also included a decomposition of relative permeability for the gas phase, which is expressed by the effective saturation using a maximum and minimum degree of saturation, i.e., $S_{\text{effective}} = (S - S_{\text{min}})/(S_{\text{max}} - S_{\text{min}})$.

The material permeability component is computed as a function of the porosity variations (Kozeny's law), and the retention curve is defined by the Van Genuchten model:

$$\frac{S_1 - S_{1,\text{min}}}{S_{1,\text{max}} - S_{1,\text{min}}} = \left(1 + \left(\frac{(P_g - P_1) - P_{00}}{P_{VG}}\right)^{\frac{1}{1-\lambda_{VG}}}\right)^{-\lambda_{VG}} \tag{1}$$

where P_g, P_1 are the gas and liquid pressures according to Van Genuchten model; λ_{VG} is the shape function; and P_{VG} and P_{00} are the capillary pressure (where P_{00} corresponds to a finite air entry value; equation (1) valid for $(P_g - P_1) - P_{00} \geq 0$). P_{VG} is calculated as:

$$P_{VG} = P_0 \sqrt[3]{\frac{k_0}{k}} \tag{2}$$

where P_0 is the initial capillary pressure and k_0 is the initial permeability.

3. RESULTS

In this simulation triangular surfaces with a thickness of 1mm generated to closely replicate the filtration process. To accurately reflect gas injection values, the simulation utilizes measured values from test 1 and applies them to the two outermost nodes connected to the filter surface at the injection point FL903 (see Fig. 3).
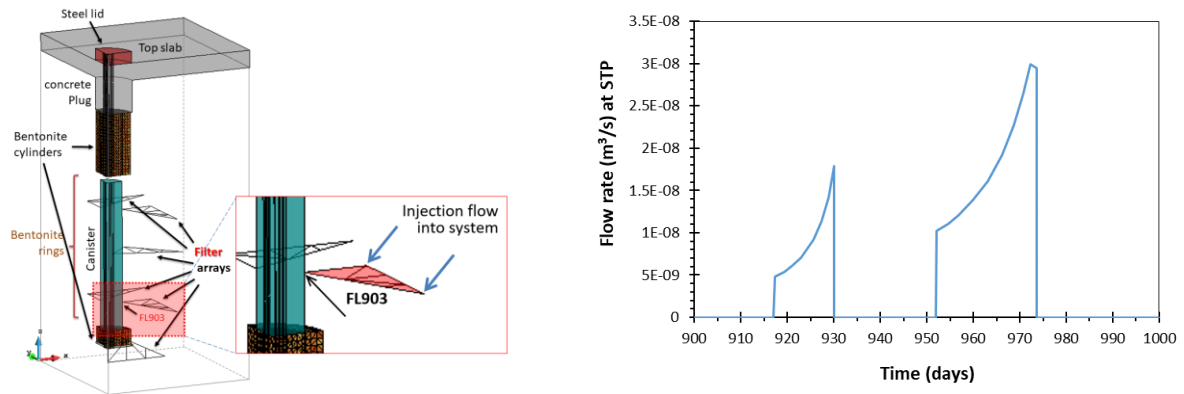
Figure 3. Modelling details: (a) filter FL903 array location detail and associated injection nodes to apply flux boundary conditions and (b) injected flow into the system in Test 1.
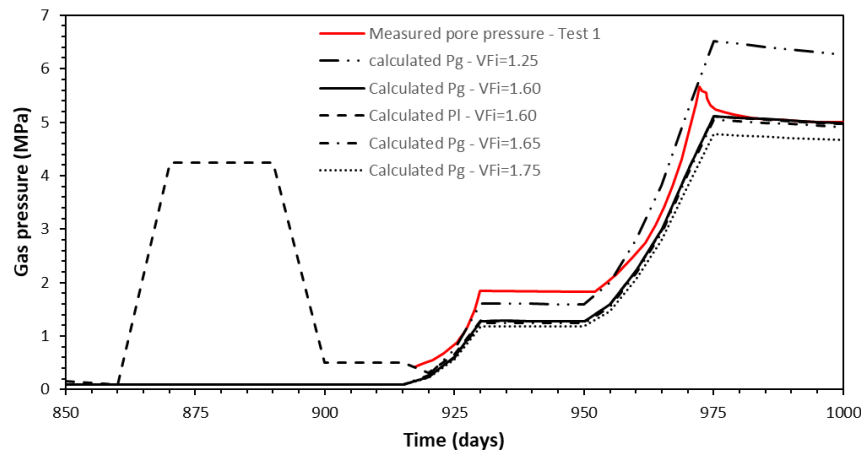
Figure 4. Calculated gas pressure modelling results for gas Test 1.

4 CONCLUSIONS

- Gas injection pressure prediction qualitatively similar to experimental measurements.
- Although the proposed model was purely hydraulic, it was able to accurately capture and predict the trend of gas evolution with great accuracy.

REFERENCES

[i] Tamayo-Mas, E., Harrington, J. F., Brüning, T., Shao, H., Dagher, E. E., Lee, J., ... & Olivella, S. (2021). Modelling advective gas flow in compact bentonite: Lessons learnt from different numerical approaches. International Journal of Rock Mechanics and Mining Sciences, 139, 104580.

[ii] Cavin, P., Gravouil, A., Lubrecht, A. A., & Combescure, A. (2005). Automatic energy conserving space–time refinement for linear dynamic structural problems. International Journal for Numerical Methods in Engineering, 64(3), 304-321.

[iii] Tamayo-Mas, E., Harrington, J., Shao, H., Dagher, E., Lee, J., Kim, K., ... & Olivella, S. (2018, June). Numerical modelling of gas flow in a compact clay barrier for DECOVALEX-2019. In 2nd International Discrete Fracture Network Engineering Conference. OnePetro.

[iv] Olivella, S., & Alonso, E. E. (2008). Gas flow through clay barriers. Géotechnique, 58(3), 157-176.

[v] Damians, I. P., Olivella, S., & Gens, A. (2020). Modelling gas flow in clay materials incorporating material heterogeneity and embedded fractures. International Journal of Rock Mechanics and Mining Sciences, 136, 104524.

[vi] Cuss, R. J., Harrington, J. F., Noy, D. J., Wikman, A., & Sellin, P. (2011). Large scale gas injection test (Lasgit): results from two gas injection tests. Physics and Chemistry of the Earth, Parts A/B/C, 36(17-18), 1729-1742.

[vii]Olivella, S., A. Gens, J. Carrera, E. E. Alonso, 1996, 'Numerical Formulation for a Simulator (CODE_BRIGHT) for the Coupled Analysis of Saline Media " Engineering Computations, Vol 13, No 7, pp: 87-112.

STRENGTH REDUCTION ANALYSIS IN POLYMERIC REINFORCED SOIL WALLS

A. Moncada[*†], I.P. Damians[*†], S. Olivella[*†] and R.J. Bathurst[§]

[*] Department of Civil and Environmental Engineering (DECA), Universitat Poliècnica de Catalunya (UPC), Campus Nord UPC, 08034 Barcelona, Spain.
E-mail: anibal.moncada@upc.edu

[†] International Centre for Numerical Methods in engineering (CIMNE), Campus Nord UPC, 08034 Barcelona, Spain. (http://www.cimne.com)

[§] Geoengineering Centre at Queen's-RMC, Civil Engineering Department, Royal Military College of Canada, Canada.

Key words: Geosynthetics, reinforced soil walls, strength reduction, polyester straps, CODE_BRIGHT.

Abstract. *The latest revision of EN-1997 allows for the use of numerical tools to design geotechnical structures, provided limit state conditions are thoroughly evaluated were analysis of the construction and post-construction stages must be included. Regarding ultimate limit state conditions, material factors must be used as to evaluate the effect of soil strength reduction on the performance of the structure. The present study focuses on the design of an idealized 10.5 m-tall reinforced soil wall with discrete concrete facing panels and polymeric strip reinforcements using finite element tools. A manual strength reduction analysis was performed, which showed no sign of structural failure, but rather hints of probable failure mechanisms which may occur, provided the structure is subjected to further unfavorable conditions.*

1 INTRODUCTION

Numerical models have proven to be reliable tools in reproducing and predicting the behaviour of reinforced soil walls (RSWs) constructed with metallic or geosynthetic reinforcements[i,ii,iii] and have been incorporated as accepted design methods in the latest version of the EN design standard[iv]. Regarding the modelling of reinforcements, it is common practice to use a single stiffness value, with equivalent parameters to account for geometric configurations, be it for 2D or 3D models. In the case of extensible polymeric reinforcement, such as polyester (PET)[v], stiffness has proven to be load-, time- and temperature-dependent. Consequently, great care must be taken when choosing a unique stiffness value. An accepted method in both numerical and analytical solutions is to obtain a stiffness modulus corresponding to, for example, 2% strain and 1000 hours[vi]. This value can be obtained from isochronous stiffness curves based on laboratory measured creep curves[vii].

Regarding the use of numerical methods as design tools, EN design standards require the verification of serviceability limit state (SLS) and ultimate limit states (ULS) for each calculated construction stage as well as end of construction conditions. For ULS verifications, the most critical failure mechanism should be studied via a strength reduction methodology.

2 NUMERICAL MODEL

Numerical simulations were carried out using the finite element program CODE_BRIGHT[viii]. The numerical model consists of a 10.5-m-tall RSW with discrete concrete facing panels placed over polymeric bearing pads (Figure 1). A concrete leveling pad was considered at the base of the parament. Reinforcement elements are modelled using continuous layer with equivalent stiffness, taking into account a configuration of four connections per panel of 2.25 m of width, with two reinforcement elements per connections. Interface elements for the soil-facing and soil-reinforcement interaction were modelled using a continuum element approach. This methodology has been successfully used in RSWs finite element models in the absence of zero-thickness elements[ix,x].
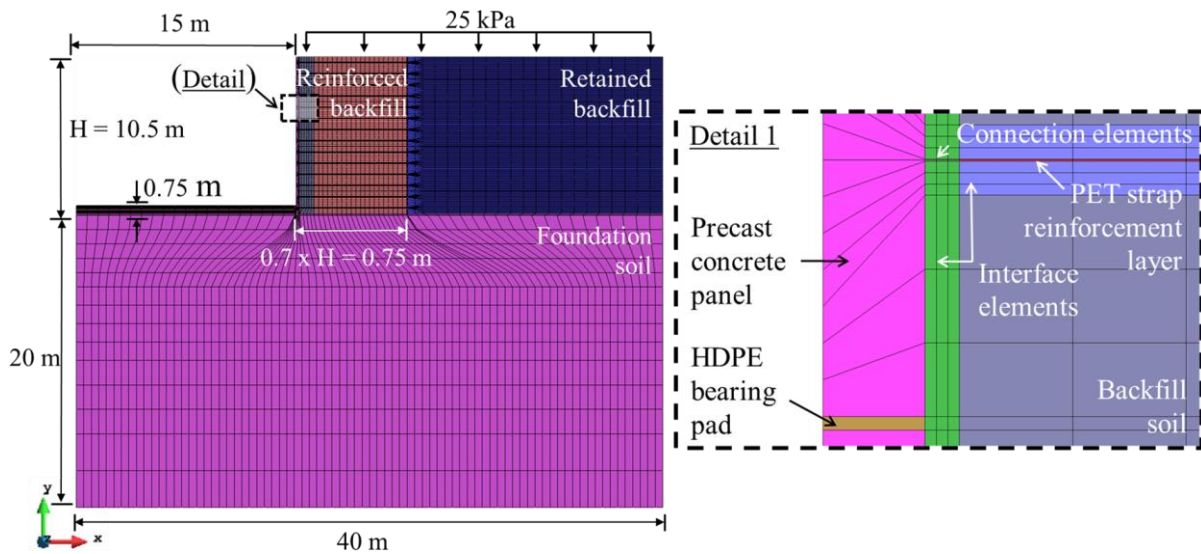
Figure 1. Numerical model mesh geometry and domain detail

The model includes a construction process consisting of, first, the construction of the foundation and leveling pad. Second, the first concrete panel is constructed. Thirdly, the first 1.5 m layer of reinforced and retained backfill material, including embedded reinforcement elements, is constructed. The placement of the next facing panel and soil layer is repeated until achieving the full wall height. A transient compaction stress of 5 kPa was considered over each soil layer. The reinforced backfill within the first 1m of the vertical wall included a reduced elastic modulus to account for a lack of proper compaction generally observed in the construction of RSW.

Soil materials (i.e., backfill, embedment, foundation, and interfaces) were modelled using an elastic-plastic constitutive model with dilatancy. Initial model parameters are detailed in Table 1, in which x is the horizontal distance to the facing and h is wall height. A reduction factor of $R_i=0.6$ was considered for the soil-facing interface. Regarding the soil-reinforcement interface, the contact area of the reinforcement strips is taken into account to calculate a representative reduction factor for the equivalent reinforcement layer, obtaining a value of $R_i=0.89$. The reinforcement elements grade (i.e., maximum tensile strength and associated stiffness) was selected as to satisfy the maximum tensions and deformations obtained by using the Stiffness method[xi] at all depths. Reinforcement corresponds to a grade 30 strap, with a stiffness value of 302 kN/strip at 2% and 1000 hours based on reliability reports of lab tested samples[xii].

Material	Parameter					
	Young modulus, E [MPa]	Poisson's ratio, ν [−]	Cohesion, c [kPa]	Internal friction angle, ϕ [°]	Dilatancy angle, ψ [°]	Density, ρ [kg/m³]
Concrete facing panel	32000	0.2	-	-	-	2300
Leveling pad	25000	0.2	-	-	-	2300
Equivalent PET strap reinforcement layer	1074	0.3	-	-	-	1890
Foundation soil	100	0.3	5	36	6	2000
Backfill soil	x <1 m: 20 / x >1 m: 10	0.3	1	38	8	1890
Soil-facing interface	4.02	0.45	0.6	25.1	0	1890
Soil-reinforcement interface	x <1 m: 20 / x >1 m: 10	0.45	0.89	34.8	8	1890
Bearing pads	h >6 m: 3.3 / h <6 m: 6.6	0.01	-	-	-	1090

Table 1. Initial model parameter values for soil and structural materials.

3 METHODOOGY

The strength reduction analysis consisted of a reduction of cohesion (c) and the friction angle (ϕ) in all soil materials until a possible failure mechanism was detected or serviceability requirements are not met. For ULS verifications, EN design standard specify a material factor of γ = 1.25, which must be applied at every construction stage, as detailed in Equations 1 and 2, where γ is the material factor, c_{soil} and ϕ_{soil} are the baseline cohesion and friction angle of the soil material, and c_r and f_r are the reduced cohesion and friction angle values

$$\gamma\, c_r = c_{soil} \tag{1}$$

$$\gamma\, tan\,(\phi_r) = tan(\phi_{soil}) \tag{2}$$

If no failure over the soil or structure is obtained, the verification is deemed completed. For internal stability, failures can occur in RSW when the reinforced soil surpasses a 2% to 3% strain threshold[xiii]. For the present study, reduction of soil strength parameters was not limited to 1.25 as to better observe the development of possible failure mechanism in the structure.

4 RESULTS

Figure 2 shows the calculated shear stresses and horizontal displacements for the base case and γ = 1.33 case. As soil strength is reduced, a gradual increase in shear stresses is observed (Fig. 2a), from close proximity to the vertical wall footing and upwards. The shear increments follow a similar trajectory than the theorical failure line, defined as 45°+ϕ_{soil} for extensible reinforcements, marked by the dotted line in the figure. No increments in shear stresses at the base of the wall suggest that no bearing capacity failures are to be expected.

Horizontal displacements show a clear bulging towards the lower half of the wall. Displacements are most predominant near the facing elements, particularly within the third compaction layer (Fig. 2b). The considered PET strap reinforcements are on the stiff side of geosynthetic materials, consequently, modelled horizontal deformations did not surpass 25 mm, or under 0.3% of the structure's height even with substantial reductions in strength.
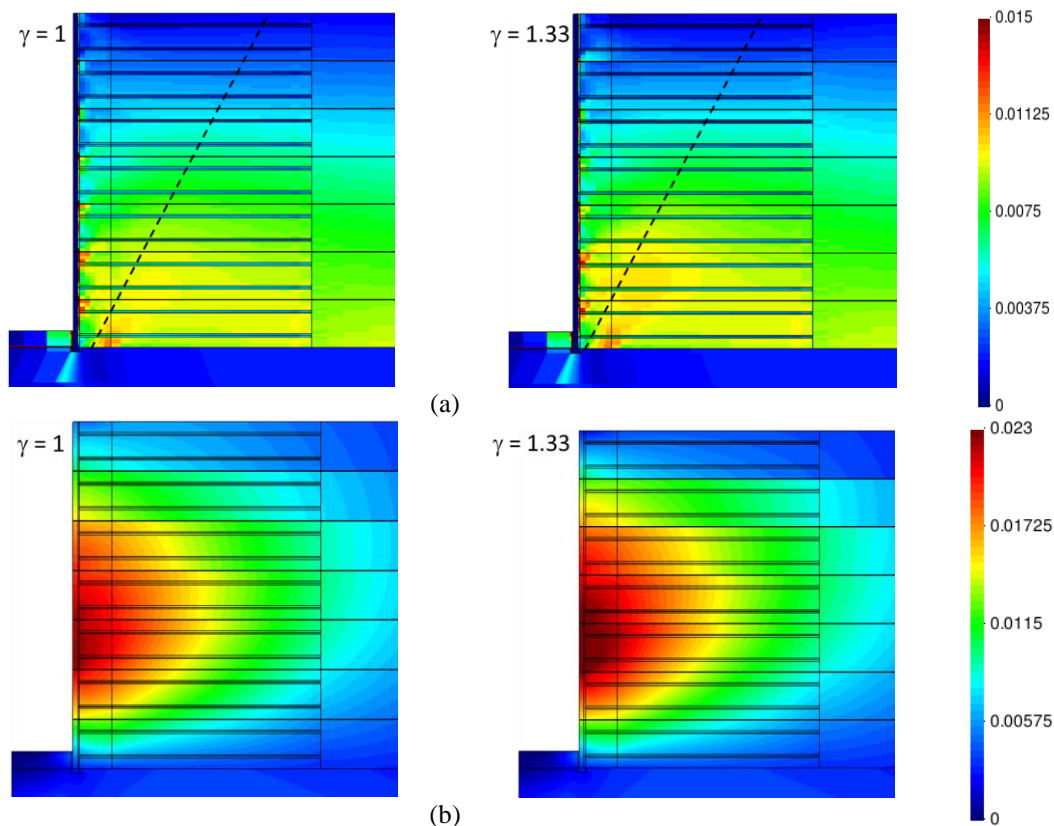
Figure 2. End of construction results for (a) deviatoric strains [-] and (b) and outward horizontal displacements [m] with initial model parameter values (left) and reduced values (γ = 1.33) (right).

Having stiff segmental panels, as soil strength is reduced, incremental horizontal displacements are noticeable at each panel connection in addition to a tilting (Fig. 3a). The relative displacement between panels is most critical between the second and third panel. For elements above, displacements indicate a behaviour more in line with a rigid block, displacing together, rather than individual movements. Displacement results suggest a developing failure zone within the third and fourth facing panels. Displacements at the base of the structure remain somewhat unchanged throughout the analysis, meaning no sliding failures should occur.

Figure 3b compares the calculated maximum stresses for each reinforcement layer using the Stiffness method against modelled results for the base case and γ = 1.33 case. As soil strength is reduced, deformation increases, thus, the load at each reinforcement layer is increased. Most noticeable variations were observed from the third to the sixth layers, corresponding to the second and third facing panel, on which the largest outward displacements occur. Except for the second uppermost reinforcement layer, modelled values are well under calculated values. As calculated values are within the 10% of reinforcements maximum tensile strength (i.e., 34.1 kN/strap), failure by reinforcement rupture is not expected.

Overall, no global stability issues were observed (i.e., sliding, overturning, and bearing capacity). Strength parameters were reduced up to a material factor of γ = 1.33, after which, convergence issues began to arise, even though there was no hint of a probable imminent failure. The later can attributed to RSWs being large deformation problems, in which the soil is expected to present significant displacements, particularly with extensible reinforcements,

which can hider finite element analysis were small strains are initially assumed. The calculated results indicate that a probable failure mechanism should be internal soil failure. For a value of $\gamma = 1.25$, no structural failure or exceeding deformations were observed at any construction stage.
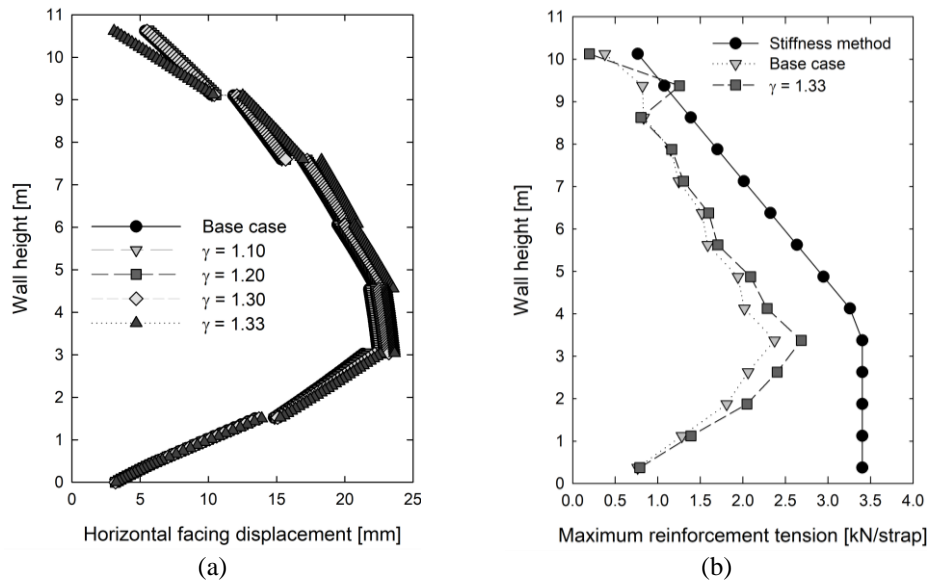
Figure 3. Comparison of (a) front facing horizontal displacements [mm] as material factor (γ) increases and (b) maximum tension [kN/strap] obtained using the stiffness method, base case model and $\gamma = 1.33$ case.

5   CONCLUSIONS

- A manual strength reduction analysis was carried out for an idealized 10.5-m-tall polymeric RSW following the requirements of the new prEN design standards.
- RSW don't have a clear failure mechanics, but rather include various internal and external stability checks which must be accounted for.
- Evidence of global instability was not observed for sliding, overturning, and bearing capacity failures.
- Modelled shear strains suggest a probable internal failure mechanism, following the theorical maximum tension line defined as $45°+\phi_{soil}$ starting from the base of the wall.
- Development of horizontal displacements suggest a probable internal failure toward the facing of the structure between 3 and 6 m of height.
- RSWs are large deformation problems, particularly when considering extensible reinforcements. Said behaviour can increase the difficulty of analyzing failure mechanisms with finite element tools with small strain assumptions. Nevertheless, the software is capable of calculating the proposed structure and infer probable failure mechanisms.

REFERENCES

[i]   Damians, I.P., Bathurst, R.J., Josa, A., Lloret, A., 2014. Numerical study of the influence of foundation compressibility and reinforcement stiffness on the behavior of reinforced soil walls. International Journal of Geotechnical Engineering, 8(3), 247-259.

[ii]   Huang, B., Bathurst, R.J., Hatami, K., 2009. Numerical study of reinforced soil segmental walls using three different constitutive soil models. Journal of Geotechnical and Geoenvironmental Engineering 135 (10), 1486–1498.

[iii]   Yu, Y., Bathurst, R.J., Miyata, Y., 2015. Numerical analysis of a mechanically stabilized earth wall reinforced with steel strips. Soils and Foundations, 55(3), 536-547.

[iv]   prEN 1997-3. 202x. Eurocode 7: Geotechnical Design — Part 3: Geotechnical Structures. F.E. with agreed CRs (v2022:5). Technical Committee CEN/TC 250 "Structural Eurocodes".

[v]   Miyata, Y., Bathurst, R.J., Allen, T. M., 2018. Evaluation of tensile load model accuracy for PET strap MSE walls. Geosynthetics International, 25(6), 656-671.

[vi]   Allen, T.M., Bathurst, R.J. 2019. Geosynthetic reinforcement stiffness characterization for MSE wall design. Geosynthetics International, 26(6), 592-610.

[vii]   Bathurst, R.J., Naftchali, F.M., 2021. Geosynthetic reinforcement stiffness for analytical and numerical modelling of reinforced soil structures. Geotextiles and Geomembranes, 49(4), 921-940.

[viii] Olivella, S., Gens, A., Carrera, J., Alonso, E.E., 1996, 'Numerical Formulation for a Simulator (CODE_BRIGHT) for the Coupled Analysis of Saline Media " Engineering Computations, Vol 13, No 7, pp: 87-112.

[ix]   Damians, I.P., Bathurst, R.J., Olivella, S., Lloret, A., Josa, A., 2021. 3D modelling of strip reinforced MSE walls. Acta Geotechnica, 16(3), 711-730.

[x]   Damians, I.P., Olivella, S., Bathurst, R.J., Lloret, A., Josa, A., 2022. Modeling soil-facing interface interaction with continuum element methodology. Frontiers in Built Environment, 8, 842495-1.

[xi]   Allen, T. M., Bathurst, R. J., 2018. Application of the simplified stiffness method to design of reinforced soil walls. Journal of Geotechnical and Geoenvironmental Engineering, 144(5), 04018024.

[xii]   Hang-Won, C., Je-Goo, J., 2020. Reliability assessment of polymeric straps (FASTEN FS E) for soil reinforcement. M213-19-15189. GECO Industrial Co., Ltd. FITI Testing and Research Institute, Chungbuk, Korea.

[xiii] Allen, T. M., Bathurst, R. J., 2013. Comparison of working stress and limit equilibrium behavior of reinforced soil walls. In Sound geotechnical research to practice: Honoring Robert D. Holtz II (pp. 499-513).

LITERATURE REVIEW OF CODE_BRIGHT

I.P. Damians[*] and S. Olivella[*]

[*] International Centre for Numerical Methods in Engineering (CIMNE) and Department of Civil and Environmental Engineering, Universitat Politècnica de Catalunya·BarcelonaTech (UPC).
Campus Nord UPC, 08034 Barcelona, Spain
Email: ivan.puig@upc.edu

Key words: CODE_BRIGHT, numerical modelling, bibliometric analysis,

Abstract. *This document provides a brief review of CODE_BRIGHT's uses and citation in the literature, made through Bibliometrix tool. Citations englobe problems involving many Geotechnical Engineering applications, being the numerical analysis of unsaturated soils and energy-related topic the most frequent ones. Further systematic literature review is needed to fully capture the general CODE_BRIGHT uses in the literature.*

1 INTRODUCTION

The use of numerical simulation programs is currently extended for both scientific and commercial/business purposes in Civil and Geotechnical Engineering framework, allowing to deepen the knowledge in where traditional analytical solutions could be limited in scope. There are several commercial software following different numerical strategies (e.g., classical finite element and finite difference methodologies, but also newer ones as discrete element or point material methods, etc.). CODE_BRIGHT[i,ii] is a finite element method (FEM) computer code developed at the Universitat Politècnica de Catalunya·BarcelonaTech (DECA-UPC) and the International Centre for Numerical Methods in Engineering (CIMNE). CODE_BRIGHT solves non-isothermal multiphase flow in deformable porous media (i.e., coupled thermo-hydro-gas-mechanical problems).

This document provides a brief/preliminary review of CODE_BRIGHT's usage scope and citation in the literature. CODE_BRIGHT literature is reviewed with a deep bibliometric analysis carried out using Bibliometrix[iii] to provide a sort of CODE_BRIGHT applications state-of-the-art. Bibliometrix is a quantitative research analysis and mapping R-programming tool for bibliography. It analyses data sources, authors and documents, and conceptual, intellectual, and social structures with their relations using Scopus database input. Thematic clusters categorization and applications is done to reveal the usefulness of CODE_BRIGHT as numerical modelling tool in the Geotechnical Engineering field.

2 CODE_BRIGHT: CO-WORDING, MAIN TOPICS AND MAIN APPLICATIONS

The CODE_BRIGHT related papers expansion through keywords, tittle and abstract wording co-occurrence map is shown in Figure 1. Co-word analysis is to map the conceptual structure of a framework using the words co-occurrences in the bibliographic Scopus collection. This figure depicts a clearer picture of the citation relation among different keywords by tracking papers+keywords that have been cited together. Thus, lines represent a citation between other related paper keywords while size of nodes is related to frequency summation. Five main clusters of interrelated keywords are generated at the literature.

Figure 1: CODE_BRIGHT's related papers keyword co-occurrence.

Figure 2 presents a map in where, according to the CODE_BRIGHT co-wording citation through the time, it is possible to somehow decompose the different topics (themes in terms of CODE_BRIGHT applications) in four groups based on their Development -density- degree (*motor* or *niche* otherwise *emerging/disappearing* or *basic* themes) and Relevance -centrality- degree (*emerging/disappearing* or *niche* otherwise *motor* or *basic* themes). "Centrality" measures the degree of interaction of a network with other networks. On the other hand, "density" measures the internal strength of the network. Quadrant on the upper-left have well-developed internal ties but unimportant external ties and so, they are of only marginal/particularized importance for the field, very specialized, *niche*, and somewhat peripheral with high density but low centrality. Themes in the lower-left quadrant are both weakly developed and marginal, having low density and low centrality and mainly represent either *emerging* or *disappearing* themes. Lower-right quadrant presents themes that are important for a research field but are still under development. This lower-right quadrant contains transversal and general *basic* themes. Finally, themes in the upper-right quadrant (*motor* themes) are both well developed and important for the structure of the research field, given that they present strong centrality and high density. As shown, several themes are appearing as *niche*, being CODE_BRIGHT a representative numerical tool on researching them. These niche topics include "energy salt underground", "dam deconstruction", "hydrate production reservoirs", as well as "unsaturated soils". This last, in addition to "waste repository" analyses are in between the mean centrality and density ones, being also potential scopes and applications well developed (*motor* themes). Despite its medium density, "numerical modelling analysis" theme currently appears as the most representative -or best candidate- as *motor* one.

Figure 2: Research themes and thematic network of CODE_BRIGHT.

Figure 3 presents the most cited[iv-xi] papers regarding CODE_BRIGHT. The figure shows the referenced papers with Scopus citations larger than 100 (counted up to 25th July 2022).

Figure 3: Most global cited documents related to CODE_BRIGHT.

3   CONCLUSIONS

- The analysis conducted in this study has revealed the interest in CODE_BRIGHT, manifested by the number of scientific productions and the high impact journal publications.
- The publications production includes CODE_BRIGHT applications on a wide range of topics within the Geotechnical Engineering field, with selected themes of clearly

growing interest.

- The analysis detected niche areas of CODE_BRIGHT, but there is a lack of motor areas in where CODE_BRIGHT can increase its presence and scope.

REFERENCES

_____

[i]   Olivella, S., A. Gens, J. Carrera, E. E. Alonso, 1996. Numerical Formulation for a Simulator (CODE_BRIGHT) for the Coupled Analysis of Saline Media. Engineering Computations 13(7): 87-112.

[ii]   CODE_BRIGHT User's Guide, 2022. Department of Civil and Environmental Engineering (DECA) Universitat Politècnica de Catalunya·BarcelonaTech (UPC) and International Center for Numerical Methods in Engineering (CIMNE). https://deca.upc.edu/ca/el-departament/seccions/etcg/recerca/projectes/code_bright https://www.gidsimulation.com/news-and-events/codebright/

[iii]   Aria M, Cuccurullo C (2017). "bibliometrix: An R-tool for comprehensive science mapping analysis." Journal of Informetrics 11(4), 959-975.

[iv]   Gens, A., 2010. Soil–environment interactions in geotechnical engineering. Géotechnique, 60(1): 3-74.

[v]   Sánchez, M., Gens, A., do Nascimento Guimarães, L. and Olivella, S., 2005. A double structure generalized plasticity model for expansive materials. Int. J. Numer. Anal. Meth. Geomech. 29: 751-787.

[vi]   Gens, A; Sánchez, M; Guimarães, L Do N; Alonso, E E; Lloret, A; Olivella, S; Villar, M V; Huertas, 2009. A full-scale in situ heating test for high-level nuclear waste disposal: observations, analysis and interpretation. Geotechnique 59(4): 377-399.

[vi]   Nishimura, S., Gens, A., Olivella, S., Jardine, R.J., 2009. THM-coupled finite element analysis of frozen soil: formulation and application. Géotechnique 59(3): 159-171.

[vii]   Gens, A., Garcia-Molina, A.J., Olivella, S., Alonso, E.E., Huertas, F., 1998. Analysis of a full scale in situ test simulating repository conditions. Int. J. Numer. Anal. Meth. Geomech. 22: 515-548.

[viii] Rodríguez, R., Sánchez, M., Ledesma, A., Lloret, A., 2007. Experimental and numerical analysis of desiccation of a mining waste. Canadian Geotechnical Journal 44(6): 644-658.

[ix]   Saaltink, M.; Batlle, F.; Ayora, C.; Carrera, J.; Olivella, S., 2004. RETRASO, a code for modeling reactive transport in saturated and unsaturated porous media. Geologica Acta 2(3): 235-251.

[ix]   Vilarrasa, V., Bolster, D., Olivella, S. and Carrera, J., 2010. Coupled hydromechanical modeling of CO_2 sequestration in deep saline aquifers. Int. J. Greenhouse Gas Control 4: 910-919.

[x]   Alonso, E.E., Gens, A., Delahaye, C.H., 2003 Influence of rainfall on the deformation and stability of a slope in overconsolidated clays: a case study. Hydrogeology Journal 11: 174-192.

Applications of CODE_BRIGHT for teaching purposes in civil engineering

Sebastià Olivella

Department of Civil and Environmental Engineering (DECA), UPC Campus Nord, 08034 Barcelona. International Center for Numerical Methods in Engineering (CIMNE), UPC Campus Nord, 08034 Barcelona. sebastia.olivella@upc.edu

Teaching in bachelor and master civil engineering programs requires a variety of geotechnical aspects that are important for the professional activity. A lot of analytical solutions and methods have been traditionally explained and permit to reach the fundamentals of the problems. Foundations and retaining structures are topics that are included in geotechnical engineering courses. These courses are usually continuation of basic geotechnical courses mainly in soil mechanics. As numerical methods are incorporated in the courses, assignments may permit students to compare numerical and analytical solutions.

Shallow foundations is a topic that contains a number or analytical solutions to calculate bearing capacity under different situations. Limitations of analytical solutions are related to geometry of the domain and homogeneity of the soil among other aspects. An exercise that is useful from the point of view of student formation is the comparison between analytical and numerical calculations.
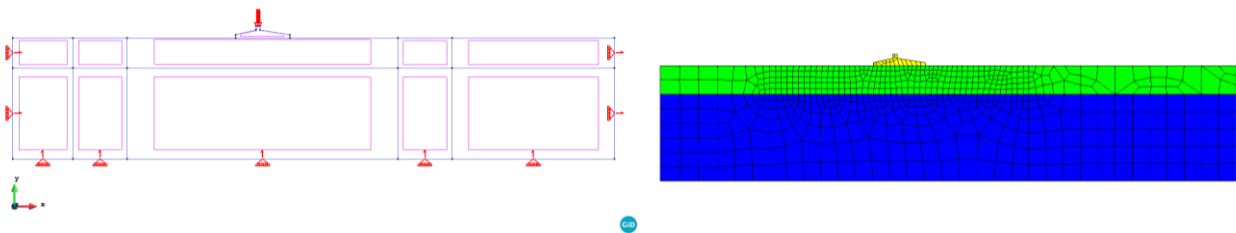
Figure 1. Model for bearing capacity for a non-simetric foundation on clay soil formed by two clay layers (0.182 and 0.104 MPa of undrained shear strength).

Figure 1 displays a model for the calculation of undrained bearing capacity for a shallow foundation siting on a ground formed by two layers of clay. The calculation is carried out using the undrained shear strength and under total stress assumptions. A foundation model can be used to calculate bearing capacity or to calculate a safety factor. The load applied to the foundation can be increased monotonically to reach failure. A safety factor can be calculated as the ratio of the failure force and the design force.

Figure 2 displays the displacement vectors and the contour field during failure. Since the footing is not symmetric, the response takes place oriented towards one of the sides. The stress

displacement curve can be used to compare the model with analytical solutions of bearing capacity provided that the geometry, material properties and assumptions are similar.
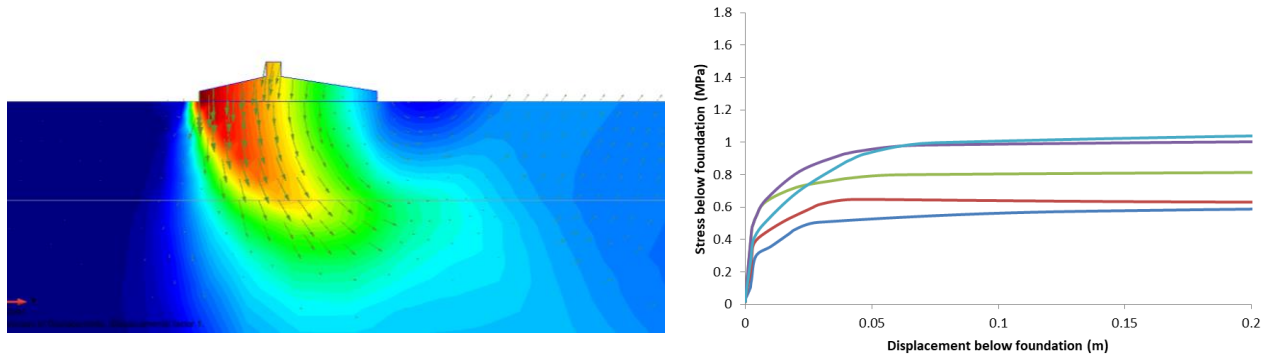
Figure 2. Results of displacements during failure and stress-displacement curves for points below the foundation.

Figure 3 is an example based on the failure of a retaining wall. The domain represents the 2D section of a slope where a road needs to be developed using a retaining wall. The retaining wall is supposed to be constructed with rockfill and is surrounded by an interface material. Stability can be calculated analytically with the traditional calculation of safety factors against overturning, sliding, foundation failure or global failure. These safety factors are based on the theories of Coulomb and Rankine for the calculation of active and passive earth forces or pressures.
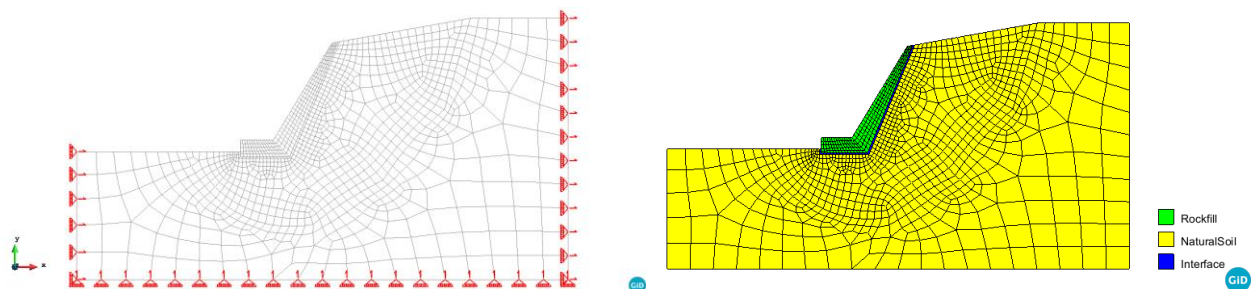
Figure 3. Retaining wall geometry, mesh and materials.

A numerical model is not used to calculate the forces caused by the terrain on the structure. In contrast, the numerical model has additional advantages like for instance the deformability of the terrain or the elastoplastic behavior of the retaining wall.

Figure 4 displays how failure is reached by strength reduction method. A safety factor can be calculated by the ratio between the strength and the reduced strength that produces failure. The method of strength reduction is an interesting alternative for the calculation of a safety factor for this type of geotechnical structures that do not have external loads, actually the only existing load corresponds to self-weight (i.e. gravity). In this method strength is reduced progressively until

failure is reached. The graph in figure 4 displays the displacement as a function of strength (the parameter M is a function of friction angle). The safety factor is determined as:

$$SF = \frac{actual\_strength}{failure\_strength} = \frac{M}{M_{failure}} \tag{1}$$
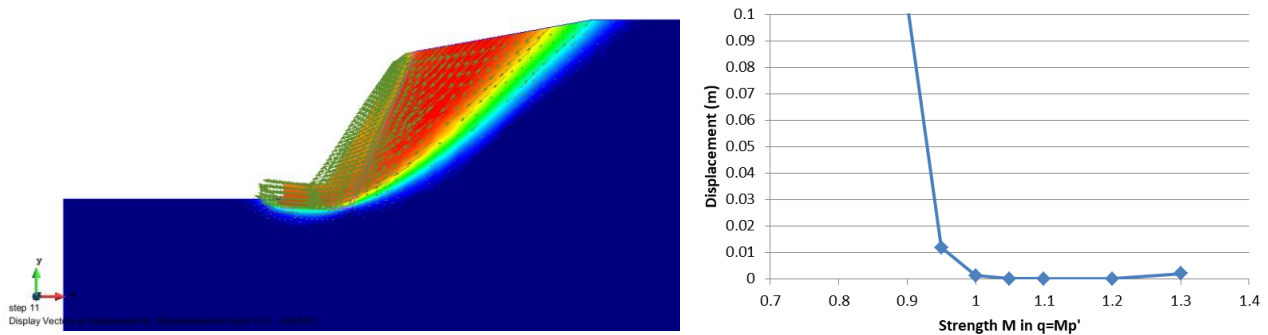
Figure 4. Retaining wall for a road in a slope. Displacement distribution during failure, and displacement versus strength for the strength reduction method.

An advantage of this method is that, it is not necessary to propose failure mechanisms for the solution of the safety factor. The deformation of the wall close to failure can be used to visualize what the dominant failure mechanism is.

The use of the assignments using CODE_BRIGHT has started and will continue in the future. CODE_BRIGHT is not professional software from the point of view that it is not prepared to carry out calculations at the level of a consulting company. But it can still be used to teach concepts that an engineer can find in more professional software that can be licensed for engineering calculations and design.

It is important to teach methodologies such as verification that the software one uses does what is supposed to do. For this it is necessary to compare with analytical solutions by performing calculations under the same assumptions. The strength reduction method is implemented in some software to carry out safety factor calculations. These can be compared with analytical calculations leading to the discussion of the predominance of the mechanisms that undergo during failure.